MODELING AND EXPLORING BATTERY MANAGEMENT STRATEGIES FOR USE OF $LiCoO_2$ LITHIUM POLYMER CELLS IN COLD CLIMATES

By

Isaac D. Thompson, B.S.

A Thesis Submitted in Partial Fulfillment of the Requirements

for the Degree of

Master of Science

in

Electrical Engineering

University of Alaska Fairbanks

May 2018

APPROVED:

Richard Wies, Committee Chair
Dejan Raskovic, Committee Member
Orion Lawlor, Committee Member
Charlie Mayer, Chair
Department of Electrical and Computer Engineering
Douglas Goering, Dean
School of Engineering and Mines
Michael Castellini,
Dean of the Graduate School

Abstract

Thesis Title: MODELING AND EXPLORING BATTERY MANAGEMENT STRATEGIES FOR USE OF $LiCoO_2$ LITHIUM POLYMER CELLS IN COLD CLIMATES

As the use of batteries to power vehicles becomes more common, a robust battery management system becomes necessary to monitor and maintain the batteries. Cold weather places a further burden on this system especially in small electric vehicles such as snowmobiles where it is desirable to use every bit of available energy from the battery cells. The problem with current battery management technology is that use of batteries in cold temperatures is often not addressed. The objective of this research was to develop an appropriate model of a lithium polymer cell with a cathode comprised of $LiCoO_2$ and develop an optimized charge/discharge method taking into account the effects of extreme cold weather and cell state of charge imbalance. A cell model was adapted and tuned that accurately captures the dynamics of a lithium polymer cell when discharged at temperatures below freezing. The model results were verified against cells discharged in an environmental chamber, which allowed accurate control of ambient temperature. Multiple scenarios were explored, looking at the effects of ambient temperature, cell initial temperature, internal heating, battery pack insulation, and how rapidly the cells were discharged. The results of the optimized battery management strategies showed improvements in the energy delivery capability of lithium polymer battery packs for small vehicles operating in extreme cold environments. In addition, this research extended the $LiCoO_2$ model down to -20 °C using validated data, showed that perceived cell capacity loss at low temperatures is primarily due to increased internal resistance, demonstrated that measured cell terminal voltage can rise under load at low temperatures, and showed that increasing the capacity of a battery pack has a better than linear gain in usable energy versus increased battery capacity. I.e., doubling battery pack capacity will more than double the useable range of the vehicle.

Preface

Much of the inspiration behind this research was a project to design and build a snowmobile capable of operating entirely from a battery electric source. This snowmobile was meant to be used in Greenland during the summer months in daily temperatures between -40 °C and -10 °C.

Because of size and weight restrictions, as well as minimizing cost, "hobby" lithium batteries were chosen. These cells are often comprised of a $LiCo0_2$ chemistry and have an exceptionally high power to weight ratio and energy density. A drawback of using this cell chemistry is that it is not formulated for best performance at sub-freezing temperatures. Therefore, a battery management system was necessary that would keep track of cell temperature and charge level. Many of the battery management systems available are not designed around using the battery in freezing climates. Many are designed to limit power when the cell temperature is too high, or to disable the battery completely if the temperature is too low. For this project it was highly desirable to have a management system which could better account for the effects of cold on the battery and react accordingly.

In order for the battery management system to accurately monitor and control the cells during subfreezing temperatures, it was necessary to know what effects the cold will have on the cells. These effects include changing the cell energy capacity, terminal voltage, and internal resistance. Temperature monitoring boards were constructed that allowed for monitoring cell temperature and location in the battery pack, as well as monitoring the connection status to parallel-connected cells. A circuit board was also developed using a battery monitoring integrated circuit (IC) which read and displayed the vehicle speed, battery current, and cell voltages on an LCD touch-screen.

Cold weather effects on the operation of lithium-based cells can also be overcome using insulation, a sealed polycarbonate enclosure and layer of fireproof material in our case. While the electric snowmobile was used in Greenland at -40 °C with no ill-effects on the batteries, more insulation could have been used to keep batteries at a safe operating temperature, while reducing load to limit higher temperatures.

The results of this project clearly illustrated the need for further study into the cold climate operation of lithium-based batteries, the topic of this thesis.

Table of Contents

Page

List of Figures

Page

List of Tables

Page

List of Appendices

Page

List of Abbreviations and Terms

Ah: Ampere-hour, the product of current in amps, and time in hours. 1 Ah is equal to 1 amp sustained for 1 hour, or 2 amps for 0.5 hours, etc.

ATV: All-Terrain Vehicle, such as a quad, 4-wheeler, or other small off-road vehicle.

BMS: Battery Management System, monitors cell voltages and temperatures and tracks remaining usable energy of battery pack.

C-rate: A measure of how fast a cell is discharged, normalized by the cell capacity. A C-rate of 1 (written as 1 C) refers to a cell being discharged from 100% charged to completely discharged in 1 hr. A rate of 20 C discharges the same cell in 1/20 of an hour, or 3 minutes. A Not to be confused with °C.

IC: Integrated Circuit, for example a MOSFET or microcontroller.

LUT: Look-up Table, often 2-dimensional but can be n-dimensional. Provides an output value given n input values.

NREL: National Renewable Energy Laboratory.

OCV: Open Circuit Voltage, the voltage measured at the terminals of a cell or battery, with no loads attached. Volt-meters and other voltage measuring devices are not considered to be loads.

SOC: State of Charge, a measure of remaining energy capacity, with 1 being fully charged and 0 being completely discharged. Analogous to % of fuel remaining in a vehicle fuel tank.

Wh: Watt-hour, the product of power in watts, and time in hours. 1 Wh is equal to 1 watt sustained for 1 hour, or 2 watts for 0.5 hours, etc.

Chapter 1: Introduction

1.1 Purpose

The over-arching goal of this research is to eventually build an all-electric snowmobile or all-terrain vehicle (ATV) capable of traveling 20-30 miles between charges in cold climates, powered by nothing more than batteries. In order to do this, a battery management system (BMS) must be developed which will allow the batteries to operate within their designed safe voltage range, while also allowing them to operate at ambient temperatures near the bottom of their specified range.

1.2 Objectives

In keeping with the over-arching goal, as well as gaining a better understanding of $LiCoO_2$ and lithium polymer cells in general in order to improve the range, functionality, efficiency, and usability of small electric vehicles in cold climates, the objectives of this thesis are:

1. Develop an appropriate model of a lithium polymer $LiCo0_2$ cell for cold temperatures.
   a. Implement an appropriate model topology. Many cell model topologies exist. A topology will be implemented which gives a sufficient level of cell behavior detail for cold climate battery use.
   b. Develop specific curves relating open-circuit voltage (OCV) and state of charge (SOC). For a resting cell, not under load, OCV can be a good indicator of the SOC. A table will be developed relating SOC and OCV.
   c. Relate cell temperature to OCV at known SOCs. Cell temperature is believed to have an effect on OCV for a given charge level. This will be explored and verified.
2. Test actual lithium polymer $LiCo0_2$ cells at various low temperatures in an environmental chamber in order to:
   a. Validate the developed model for cold temperatures.
   b. Explore self-heating of batteries at low temperatures. As cells are discharged at low temperatures, high internal resistance causes the cells to gain heat. This will be explored to determine an optimal discharge strategy which maximizes useful energy extracted from the battery pack
3. Explore various use scenarios of small electric vehicles using the validated model.

1.3 Existing Battery Technology

There are many existing battery technologies available today, and each of them has their own advantages and disadvantages. This thesis will not cover other similar means of energy storage such as fuel cells or super capacitors. On a very broad scale, there are two main categories of batteries; primary [1], or non-rechargeable batteries, and secondary [2], or rechargeable batteries. Primary batteries include alkaline batteries such as the common AA and AAA formats, as well as most button cell watch batteries.

The other main category of battery is the secondary battery. Today, secondary batteries are far more common than primary batteries due in large part to their being cheaper to use over the life of the battery. While primary batteries still find use in devices which require a long shelf life with no chance to recharge [3], most batteries used today are of the rechargeable type.

In the secondary category, there are several main types of batteries in use today. One of the most common and well known is the lead acid battery [4], used in almost every automobile as well as most airplanes and many home battery banks. Lead acid batteries have several advantages over other chemistries which has kept them in regular use. The first advantage is cost: lead acid manufacturing plants are still more numerous than other battery chemistries, making them cheaper to produce for the time being. Second, lead acid batteries require very little maintenance or management; charging them is usually as easy as applying a dc voltage to the main terminals [5], and the cells will self-balance while charging. Resistance also increases greatly as the battery charges; the result of which is that charging is mostly self-limiting. As the battery nears full charge, the resistance of the cells increases, decreasing the current flowing through the battery.

Nickel-Cadmium, or NiCd [6], batteries, are commonly used for cordless tool applications, although their use is rapidly declining in all but the cheapest tools, being replaced by lithium-based chemistries.

Nickel metal hydride, or NiMh, batteries have been and are currently used in many electric and hybrid vehicles [7], notably GM's EV1 and the Toyota Prius, respectively. Compared to NiCd, NiMh batteries maintain a higher power output throughout the discharge cycle. This means that the device the battery is powering is able to provide nearly the same performance

with a partially discharged battery as with a fully charged battery. NiMh briefly replaced NiCd as the battery of choice in radio control model hobby applications, but has mostly been replaced by lithium-based batteries in recent years.

While there are many other battery chemistries which could be touched upon, the predominant cell chemistry type and the one that will be explored in this thesis is the lithium battery. Lithium batteries as a family exhibit very high energy density and power density, a very flat discharge curve (again, meaning almost no difference in performance between fully charged and discharged), and do not exhibit any "memory" [8] when recharged before fully discharging them.

In the lithium family, there are yet again many different types [9], but the two most common are lithium iron phosphate ($LiFePO_4$) and lithium ion. In general, $LiFePO_4$ cells are higher capacity and form factor, and are commonly used in larger applications such as solar photovoltaic battery energy storage systems or large electric vehicle batteries. Lithium-ion batteries are generally smaller format cells and are commonly used to power cell phones, laptops, modern cordless tools, and many newer electric passenger vehicles.

Included in the lithium-ion family are lithium polymer (or LiPo) cells. There is no chemical difference between Li-ion and LiPo batteries: the difference is in how they are constructed. In a typical Li-ion cell, the anode and cathode are sandwiched together with a porous insulator between them, rolled into a tight cylinder, and then fit inside a cylindrical metal case. An illustration of this is shown in Figure 1-1. This is what makes up many laptop batteries, by stacking 6 to 12 of these cells together and enclosing them in a sturdy plastic housing. The newest laptop battery technology takes advantage of the thinner form factor of LiPo cells, discussed next.

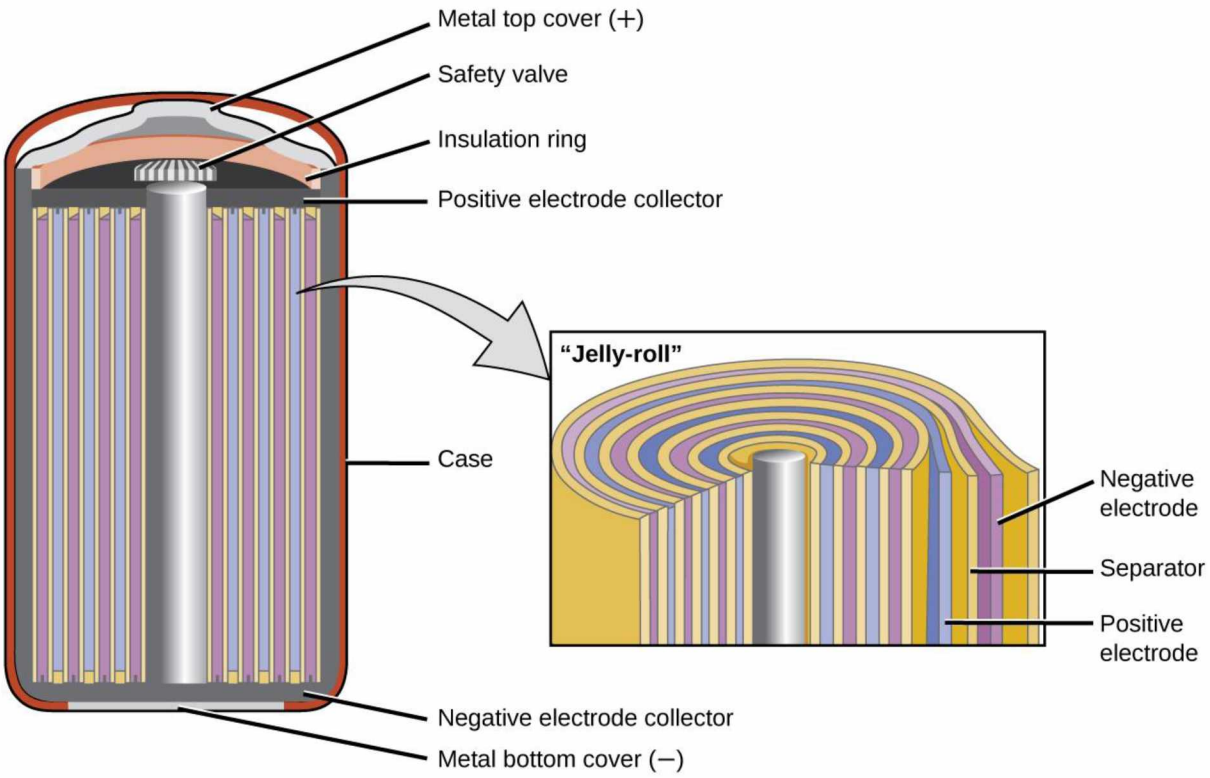

Figure 1-1: Physical construction of typical metal canister lithium cell. Taken from [10].

In a LiPo cell, the same anode, cathode, porous insulator sandwich is built up, but this time it is folded and stacked instead of rolled, and then enclosed and vacuum sealed in a polymer pouch. The main benefit of the LiPo cell versus the Li-ion cell is that the flat, rectangular shape of the pouch cell lends itself to a higher spatial energy density than the cylindrical shape of the Li-ion cells. An example of a typical LiPo pouch cell is given in Figure 1-2.

Figure 1-2: Typical LiPo pouch cells comprised of copper and aluminum electrodes sandwiched with an insulating polymer and sealed in a foil polymer pouch.

Even in the LiPo group, there are at least six distinct battery chemistries, and each of them has advantages and disadvantages. Given in [11] these chemistries are as follows. Lithium cobalt dioxide, or $LiCoO_2$, cells have a high specific energy (making them ideal for devices that require long run times), but have a relatively shorter cycle lifetime and lower specific power. Lithium manganese oxide, or $LiMn_2O_4$, cells have a very high specific power, making them capable of charging and discharging very quickly at the expense of capacity. Cells utilizing pure manganese are no longer commonly used, and have been replaced by lithium nickel manganese cobalt oxide, or $LiNiMnCoO_2$, cells. A convenient feature of these cells is the chemistry can be modified by changing the percentage of nickel and cobalt to achieve a desired balance between energy and power capacity. Lithium iron phosphate, or $LiFePO_4$, cells have a lower specific energy and power than most other lithium chemistries, but are also one of the safest lithium battery technologies and are more tolerant of extended periods of overcharging or under charging.

Lithium nickel cobalt aluminum oxide, or $LiNiCoAlO_2$, cells have a very high specific energy and good specific power as well as a long cycle life. Their drawbacks are cost and safety. Finally, lithium titanate, $Li_4Ti_5O_{12}$, is a relatively older lithium battery technology, dating back to the 1980's. It has a very high charge and discharge rate, as well as excellent low-temperature energy capacity, retaining 80% of its energy capacity at -30 °C. Its primary disadvantage is a low energy density.

1.4 Specific Battery Chemistry in this Thesis

The chemistry that will be explored in detail in this thesis is $LiCo0_2$, also called lithium cobalt oxide, or just LCO. Because there are many varieties of LCO, the specific cell this research focuses on is designated "Nano-Tech" manufactured by Turnigy and has a 65-130 C-rate.

The biggest advantages of LCO cells versus other lithium-based chemistries is their high energy density, moderate cost, and high availability [12]. In keeping with the goal of this thesis, it was decided to focus on a cell which would be a good candidate for small to medium sized electric vehicles. Given that the largest contributor to weight in most battery electric propulsion systems is the battery, and the relative light weight of the vehicles of interest, it is important that the battery selected be as light as possible for a given amount of energy capacity.

While there are other lithium chemistries which may be more suitable as electric vehicle batteries, the choice was made to focus on a chemistry which was affordable and obtainable. Besides costing less than many competing lithium chemistries, LCO has the distinct advantage of being obtainable off-the-shelf at almost any hobby shop or easily ordered from hobby supply sites. By focusing on a cheap, available battery chemistry, this thesis aims to model cold-climate battery operation in small to medium vehicle applications and real world scenarios.

1.5 Development of $LiCoO_2$ Model

Many cell models exist, but each falls short in some way. This research deals specifically with lithium polymer pouch cells at very low temperatures. In reviewing the current literature on this topic, no validated and tested models for lithium polymer cells in extreme cold climate applications were identified. In this thesis, a pouch cell refers to a form factor of cell made up of

rectangular plates of alternating anode and cathode material separated with a zig-zag folded insulator and sealed inside a polymer pouch. The other main type of lithium polymer cell is the familiar cylindrical shape where the anode, insulator, and cathode are rolled together and sealed in a cylindrical steel canister. For reference, a typical pouch cell is shown on a previous page in Figure 1-2. A diagram of the internal assembly of a pouch cell is shown below in Figure 1-3.

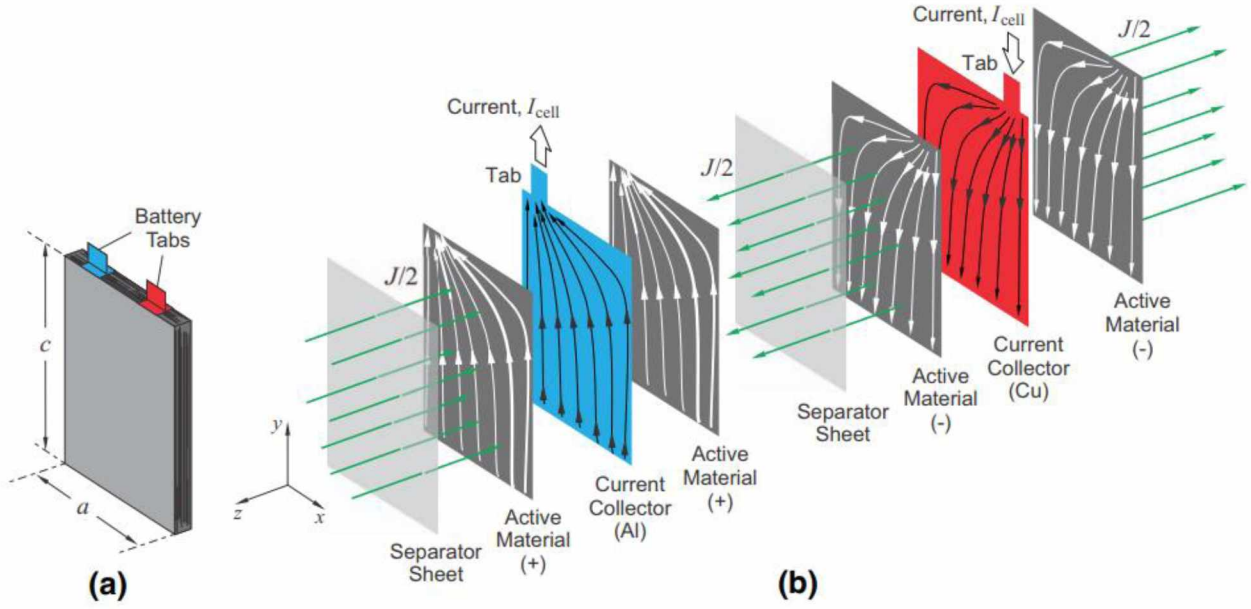

Figure 1-3: Diagram of construction of pouch cell, taken from [13].

The National Renewable Energy Laboratory (NREL) has done extensive testing of various cell models, however, less attention has been paid to analyzing performance in cold climates. In [14] the authors take into account the temperature-dependent components of a typical lithium-based cell, but do not specifically address $LiCoO_2$. Additionally, preliminary laboratory testing, as well as manufacturer data sheets, indicate that there are many different varieties and compositions of cells even within the $LiCoO_2$ category. For these reasons, it is desired to construct and test a model which specifically addresses cells designated "65 – 130 C-Rate," manufactured by Turnigy.

1.6 Expected Results

It is expected that this research will result in a better understanding of lithium polymer pouch cells at low temperatures (between 0 °C and -40 °C) and, by extension, a better correlation

between cell voltage and true SOC. This will enable use of these cells in snowmobiles, ATV's and other vehicles used in extreme cold climates. This, in turn, will enable the design of more optimized battery management schemes for lithium polymer pouch cells in cold climate applications.

1.7 Background Research

1.7.1 Current State of the Art

Current research into the state of the art in BMSs for lithium polymer batteries involves accurately estimating SOC, maintaining equal state of charge between all cells in the pack, and investigation into how much effect temperature has on the cells.

1.7.2 State of Charge (SOC) Estimation

One very important function of any good BMS is its ability to accurately estimate current SOC. This is important because distance-to-empty and maximum current draw are both affected by SOC. A fully charged battery pack will obviously be able to travel farther than a pack that is only half full. Additionally, a pack that is nearly discharged should not be discharged as hard as a pack with 30% or more remaining charge. This is partly because internal resistance of cells increases exponentially as the cells become discharged [15].

There are a number of strategies for SOC estimation, most of them generally involving either measuring the cell voltage or counting amp-hours delivered from a fully charged battery [16]. There are advantages and disadvantages of using these two general SOC estimation methods. The largest problem with measuring cell voltage is that cell voltage only changes very slightly over most of the working SOC range. For example, as demonstrated in [17] battery voltage only drops from 3.4 Vdc to 3.2 Vdc when SOC decreases from 90% to 10%. Over the working SOC range, cell voltage is much more affected by temperature [15] and load [18] than it is by SOC. Given this, cell voltage can be a useful indicator of the fully charged or fully discharged state, but is very limited for reporting accurate SOC at other points. Coulomb counting is a much better method of estimating remaining charge in a battery pack. The underlying idea is simply to measure amp-hours consumed from the pack, beginning from a known capacity. By subtracting the amount consumed, the remaining SOC is calculated. The difficulties involved with coulomb counting stem from the requirements of extremely accurate current measurements and the

inability to directly measure loss current due to internal shunt impedance. The advantage of the coulomb counting method is that amp-hour output is only slightly affected by temperature. In [15] it is shown that lithium batteries deliver nearly the same amp-hour output at low temperatures as they deliver at optimal temperatures, although at a lower voltage level.

At the forefront of SOC estimation is the use of Kalman filtering based on the OCV-SOC relationship and known hysteresis between charge and discharge voltage. This is covered in detail in [17]. Here, a $LiFePO_4$ model is developed and used to calculate the corresponding OCV based on battery pack measurements. Then, the SOC is calculated from a lookup table relating OCV to SOC.

1.7.3 Maintaining SOC between Cells

While it is important to be able to estimate the SOC of the battery pack, it is equally important to be able to estimate the SOC of every cell in a series-connected pack. This is because the useful remaining capacity will be limited by the cell with the lowest SOC [19]. To eliminate this bottleneck, it is desirable to ensure that all cells are charged to the same capacity and maintain an equal SOC over the full course of discharge. There are several approaches to this problem. The first is to simply charge each cell to the same voltage, which can be accomplished by charging the pack as a whole and then selectively discharging individual cells whose voltages are higher than the average cell voltage. This has the benefit of being fairly easy to implement, as all that is required is to measure the voltage of each cell and then switch a load resistor across individual cells to discharge them [20]. The drawback of this method is that cells can only be balanced when fully charged, because otherwise the voltage difference between cells is too small to accurately measure. Also, this method has no way to add charge to weak or low-voltage cells, which can be very desirable if the pack has one or more cells which are considerably lower in voltage than the pack average.

Instead of passive balancing, it is more effective to utilize active balancing. There are several battery management integrated circuits (ICs) just coming to market, but one of the most capable is Linear Technologies LTC680x series [21]. This IC can be used to monitor battery voltage and temperature, and can be used to communicate with and control the power electronics necessary for active balancing.

1.7.4 Open Areas Identified for Research

Based on an extensive literature review, nearly all current research being done involving batteries in vehicles is directed toward using lithium iron phosphate $LiFePO_4$ cells. Very little research has been done toward lithium polymer $LiCoO_2$ batteries for use in vehicles, more specifically in extreme cold temperatures (lower than -20 °C). Furthermore, no research was found discussing ways to limit the load on batteries until they are warmed up to operating temperatures. Temperature has a large effect on battery capability as evidenced in [22] and [23], however, these studies do not include extreme cold temperatures. Some sources report that energy density at -40 °C is only 5% of the energy density at 20 °C [22], while another source [15] looks at capacity differences between 20 °C and -20 °C, but does not look at lower temperatures. Based on this knowledge gap the point of this thesis is to investigate the use of lithium polymer batteries in extreme cold temperatures (below -20 °C).

1.8 Organization of Thesis

The rest of this thesis is organized as follows to detail research work towards developing and testing a working model of lithium polymer batteries for use in extreme cold temperatures (below -20 °C). The development of a battery model, the necessary input and output parameters, measurement techniques, and how they are used to study the performance of a battery are discussed in Chapter 2. The specific lithium polymer LiCoO2 battery model and how it best fits with low temperature conditions is described in detail in Chapter 3. Laboratory testing in a controlled environmental chamber environment, model validation, analysis to compare the battery model data to the laboratory test data, and subsequent results are discussed in Chapter 4. Finally, conclusions, as well as future improvements and research to further enhance the lithium polymer LiCoO2 battery model and management systems in cold environments are presented in Chapter 5.

Chapter 2: Modeling Lithium Polymer Batteries

2.1 Battery Models

When studying the charge and discharge characteristics of batteries, it is extremely helpful to be able to do many iterations of similar scenarios on a computer, before (or even after) taking actual measurements from cells in a laboratory testing environment. Authors in [24] and [25] discuss some of the many types of battery models which can be employed, depending on what is desired to be studied. The simplest of these models is the empirical model. An empirical battery model is an electrical representation of a cell which can be implemented with well-known circuit elements. By representing a complex chemical and thermodynamic cell as basic circuit elements, it is possible to analyze the cell using simple mathematical equations. The empirical model does not account for physiochemical effects, and as such is not suited for studying the behavior of cells that have not been built and tested yet.

Because circuit analysis and the equations governing it have been well developed, there are many existing computer programs and pieces of software which can be used to perform extensive analysis on the empirical battery model. MATLAB® and the visual modeling program Simulink®, are used extensively in [26] and [27] to model and simulate lithium ion cells. There are many advantages to using a battery model in addition to performing tests and measurements on actual cells. An obvious advantage is cost, but other advantages include ease of data collection, ability to collect large amounts of data in a much shorter amount of time, and the ability to explore scenarios which might otherwise be hard to test for in a lab environment.

There are several different commonly used battery models, depending on the chemistry being studied and the cell accuracy desired, balanced against the computing power available to analyze the model. The simplest model, called the internal resistance R_{int} model, is nothing more than a resistor in series with an ideal voltage source. Values for the voltage source U_{oc} and the resistor R_0 are implemented with lookup tables, and are functions of charge level, health of the battery, and temperature [28]. This model is shown below in Figure 2-1.

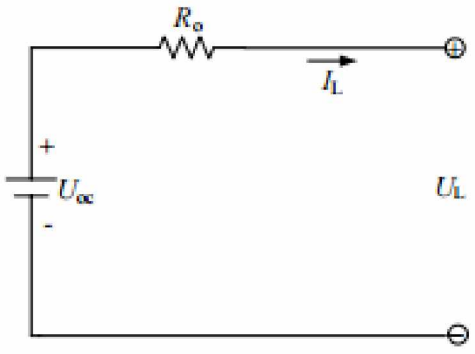

Figure 2-1: Basic internal resistance R_{int} battery cell model using a voltage source in series with a resistor [28].

The terminal voltage U_L is easily calculated using (1) given below, where I_L is the load current through the cell.

$$U_L = U_{oc} - I_L R_0 \tag{1}$$

Because of the simple topology of the R_{int} model, it is easily simulated but often not accurate enough for most work. A more accurate model, used by the SAFT Battery Company, is the RC model given below in Figure 2-2.

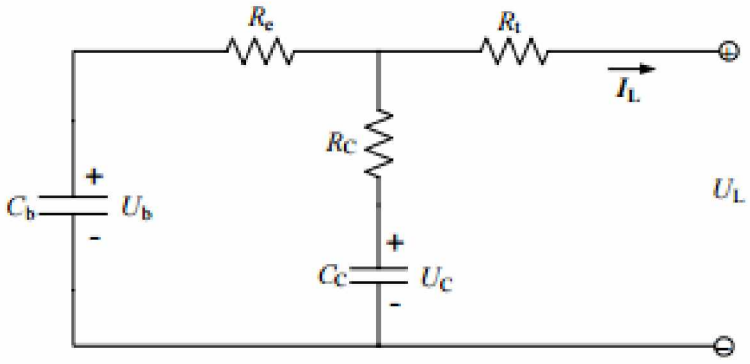

Figure 2-2: RC circuit model of battery cell [28].

The most notable differences between the RC model and the R_{int} model are that the RC model uses a very large capacitor value to represent the chemical charge storage of the battery instead of an ideal voltage source, and uses a much smaller second capacitor to help account for the surface effects of the electrodes.

2.2 Lithium-Based Battery Models

Regardless of the exact chemistry, most, if not all common lithium cells share two common model topologies. These two models are fundamentally very similar, and which one is chosen will depend on the degree of accuracy required as well as the level of computer power available for implementing the model. Both of these models are RC circuit models coupled to a voltage source. The difference between the two models is the number of series-connected RC branches used in the model, with one model using a single RC branch in series with a resistor, and the second, more complex model adding a second RC branch in series with the elements of the first model.

Shown in Figure 2-3 below is the single RC model of a lithium battery cell, also called the Thévenin cell model. Here, the open circuit voltage U_{oc} represents the voltage produced by the chemistry of the cell, and is measured at the cell terminals with no load connected. This is shared between both cell models and is functionally identical between the two. R_0 is the series ohmic resistance of the cell and represents the resistance of the wires and terminals as well as the internal connections of the cell and internal resistances of the cell. R_{Th} and C_{Th} together make up the dynamic elements of the cell model, and are responsible for the exponential decay that shows up in the terminal voltage when a pulsed load current is applied to the cell.

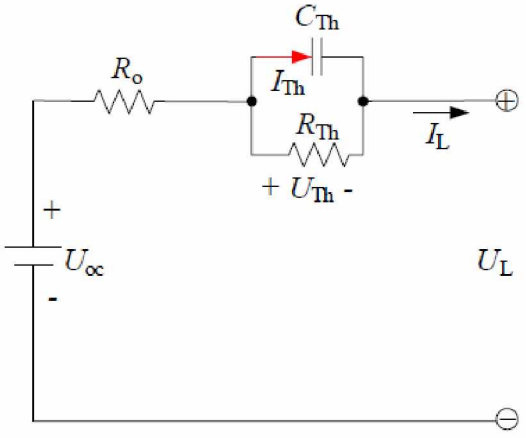

Figure 2-3: Single RC lithium battery cell model [28].

Most of the series resistance is due to imperfect conductivity of the electrolyte, as well as slow ion mobility. In lithium ion batteries, as with most cell chemistries, series resistance increases as the cell ages, eventually becoming high enough that the cell is no longer useful.

Because internal resistance is proportional to the number of charge-discharge cycles, it is a good indicator of cell life and can be used to help decide when the battery or cell should be replaced. An equation relating these can be written as

$$R_{Internal}=R_{Internal,\ Initial}+C*Y \tag{2}$$

where C is a proportionality constant and Y is the number of charge-discharge cycles. As series resistance increases, cell efficiency decreases due to a portion of the charging current being lost directly to heat. This is true of discharge current as well.

R_{Th} and C_{Th} together represent the dynamic electrochemical properties of the cell. The effect of R_0 and the parallel combination of R_{Th} and C_{Th} can most easily be observed in Figure 2-4, at the moment that the cell current makes a step increase. The cell voltage drops nearly instantly as the current is applied. This vertical drop in cell voltage is due to the voltage drop effect of R_0, and is directly proportional to the current through the cell.

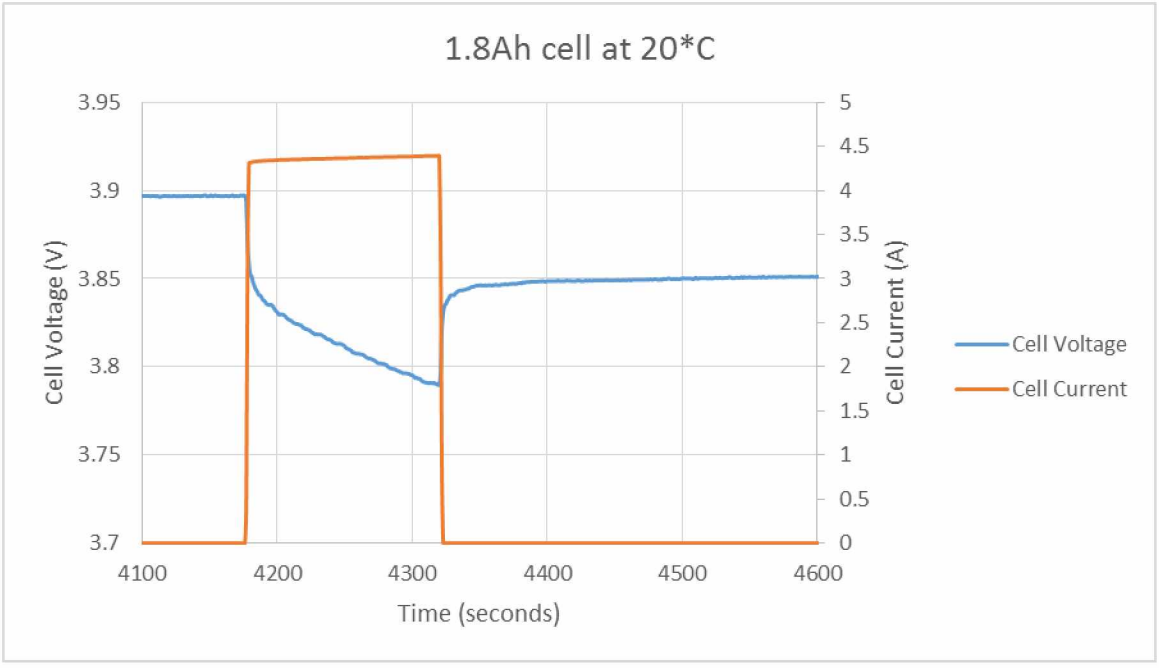

Figure 2-4: Discharge pulse of a lithium ion cell during testing in the UAF cold chamber.

Shown below in Figure 2-5 is a diagram of the effect of internal resistance in a cell, and how R_0 can be calculated [29]. In this figure, the pulse load is constant current, giving a square current pulse, where in Figure 2-4 the pulse load is constant power, resulting in a slightly increasing current pulse as the cell voltage drops. One of the simplest methods to calculate internal resistance R_0 is given in (3) below, referring to notation used in Figure 2-5.

$$R_0 = \frac{U_1 - U_2}{I_2 - I_1} \tag{3}$$

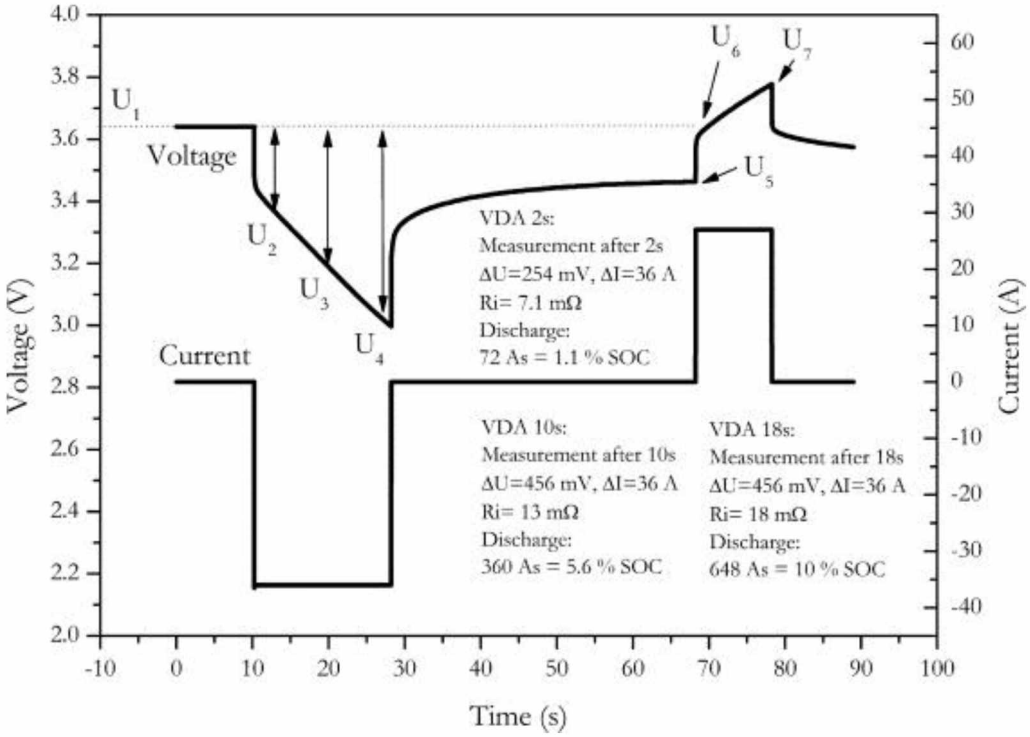

Figure 2-5: Effect and measurement of internal resistance [29].

Referring back to Figure 2-4 it can be seen that there is an exponential decay in cell voltage, becoming linear at roughly time $t = 4200$ s. The decay in cell voltage can be very accurately modeled as the effect of a parallel RC circuit being charged by a current source. This model can be seen in Figure 2-3, represented by R_{Th} and C_{Th}. The relationship between voltage and current during the current pulse due to the RC circuit can be expressed by the equation

$$\frac{U_{\text{L}}}{I_{\text{L}}} = \frac{R_{\text{Th}}}{1 + sR_{\text{Th}}C_{\text{Th}}}, \tag{4}$$

where s is the Laplace transform variable.

Common to most cell models is an electrochemical voltage source, representative of the voltage produced by the chemical reactions inside the cell. Some models refer to this as U_{oc} (where U is used instead of V to represent voltage, and OC is open-circuit.) In this thesis, models which are developed refer to this voltage as V_{oc} meaning open-circuit voltage, or E_m (indicating electromotive force of the main branch.) Referring to Figure 2-5, from approximately time t = 4200 s to 4320 s, the cell voltage drops very linearly. This linear voltage drop is due almost entirely to the internal battery voltage E_m and the relationship between E_m and SOC. As SOC decreases, E_m and the terminal voltage decrease quite linearly between 80% and 20% SOC. Finally, as the discharge current drops to zero, the cell voltage initially increases by very nearly the same amount that it first dropped (again due to R_0 and then gradually climbs and levels off, explained by R_1 discharging the accumulated energy in C_1.

Adding to the Thévenin model, the PNGV (Partnership for a New Generation of Vehicles, 2001) [26] adds a capacitor in series with the entire circuit to represent the loss of electromotive force due to discharge as shown below in Figure 2-6.

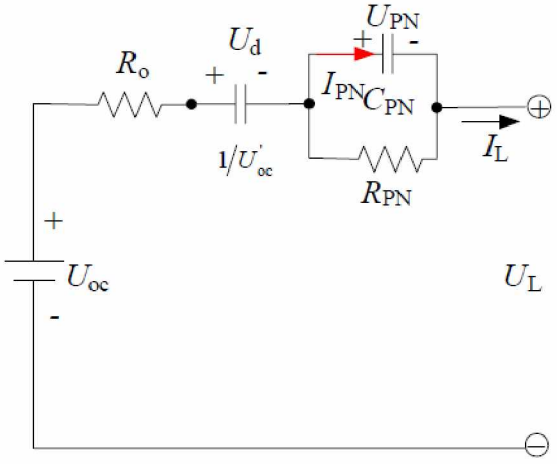

Figure 2-6: PNGV cell model using series capacitor to account for loss of electromotive force due to discharge [28].

Instead of the terminology R_{Th}, and C_{Th}, it is common to simply refer to these circuit elements as R_1 and C_1 as shown in Figure 2-7.

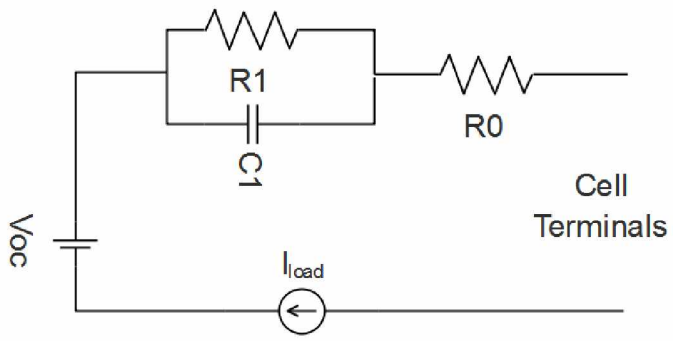

Figure 2-7: Circuit diagram of Thévenin battery cell model. Redrawn from [27] and [28].

In addition to basic circuit elements, an accurate battery cell model will take temperature and heat into account. For a DC representation, this is accomplished by first representing heat (power) produced as the product of the square of the current through the resistive elements of the cell and the resistance value of those elements,

$$P_{loss} = (I_{load}^2)(R_0 + R_1), \tag{5}$$

and secondly calculating the resulting cell temperature as a product of the heat produced and the specific heat of the cell being studied

$$T_{Cell} = T_{ambient} + P_{loss} C_p, \tag{6}$$

where T_{cell} is the (assumed uniform) cell temperature, $T_{ambient}$ is the ambient temperature around the cell, P_{loss} is the heat energy generated in the cell as calculated in (5) and C_p is the specific heat of the cell.

2.3 Model Input and Output Parameters

The model shown in Figure 2-8 uses ambient temperature and cell current as time-variant inputs. The convection heat-loss coefficient is a time-invariant input which models the amount of insulation used to insulate the battery pack or cell. Model outputs are SOC, cell voltage and cell core temperature.

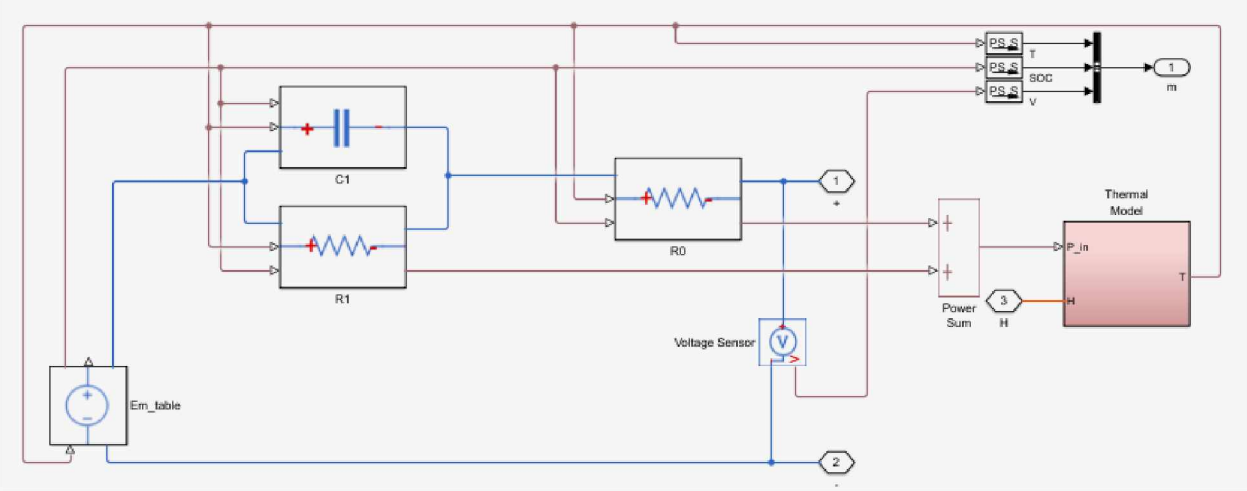

Figure 2-8: Cell model showing R_0, R_1, C_1, and E_m as well as thermal block [27].

Here, the actual values of the four components (R_0, R_1, C_1, and E_m) that make up the cell model are driven by lookup tables instead of having fixed values. This allows the component values to change based on cell temperature and SOC.

Inside the thermal block shown in Figure 2-8 is the cell thermal model, given below in Figure 2-9.

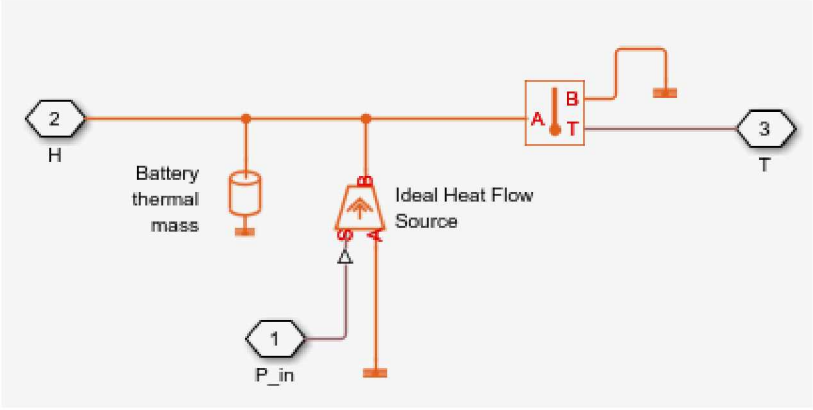

Figure 2-9: Cell thermal model showing thermal mass, heat energy input, ambient temperature input, and cell temperature output [27].

The thermal model provides a feedback loop for the cell temperature. Inside the thermal model is a thermal mass representing the specific heat C_p of the cell, as well as a heat flow source which converts that heat into a temperature rise in the cell.

2.4 Model Results

An accurate cell model can be used to predict battery behavior in varying operating conditions. It is especially useful in learning how much heat is generated by the cell at different current levels and ambient temperatures, and how much the cell voltage will be affected by a given load at a given temperature. By correlating voltage sag with cell load at given temperatures, it will be possible to accurately estimate cell SOC under most operating conditions. Model results can then be used to help intelligently manage the cells or battery pack, without having to modify or add any new hardware.

As an example, a charging strategy could be developed and optimized, to help the user decide if the battery pack should be charged just after use and then allowed to sit full, or if it should be allowed to sit mostly discharged and then charged just before use. It will also help to illustrate the effects of insulation (and amount) on the cells, and if simply insulating a battery pack is a viable means of utilizing a fully electric vehicle in extreme cold climate conditions.

2.5 Improving Lithium Polymer Battery Management Technology

The results of this thesis will be used to improve the accuracy of lithium polymer battery SOC estimates at below-freezing temperatures. By more accurately knowing the SOC, a more optimal management strategy can be employed, and in most cases will result in the battery being useful for a much longer period of time at much lower temperatures than are otherwise possible. Additionally, a better understanding of how lithium polymer batteries behave at lower temperatures will allow users to more intelligently charge and manage these packs in cold weather conditions. The cold weather lithium polymer battery model used in this thesis and environmental chamber testing methods used for determining the parameters of the model are discussed in the following chapter.

Chapter 3: Cold Weather Model of Lithium Polymer Battery

This thesis expands on a model topology developed in [12] by including real world testing at sub-freezing temperatures on lithium polymer $LiCo0_2$ cells. Here, model parameters for popular $LiCo0_2$ cells are measured with good certainty. In addition, discharge profiles have been measured and recorded at cold temperatures which could be used in future modeling work.

3.1 Model Topology

The specific model topology used in this thesis is the single RC model. Throughout testing it was determined that the single RC model adequately represented the cell behavior, while being much faster to simulate than other, more complex topologies. As previously mentioned, this topology consists of a voltage source in series with a single resistor and a parallel combination of a resistor and capacitor. In this thesis, the value of each component is driven by a 2-dimensional lookup table which accounts for temperature and cell SOC.

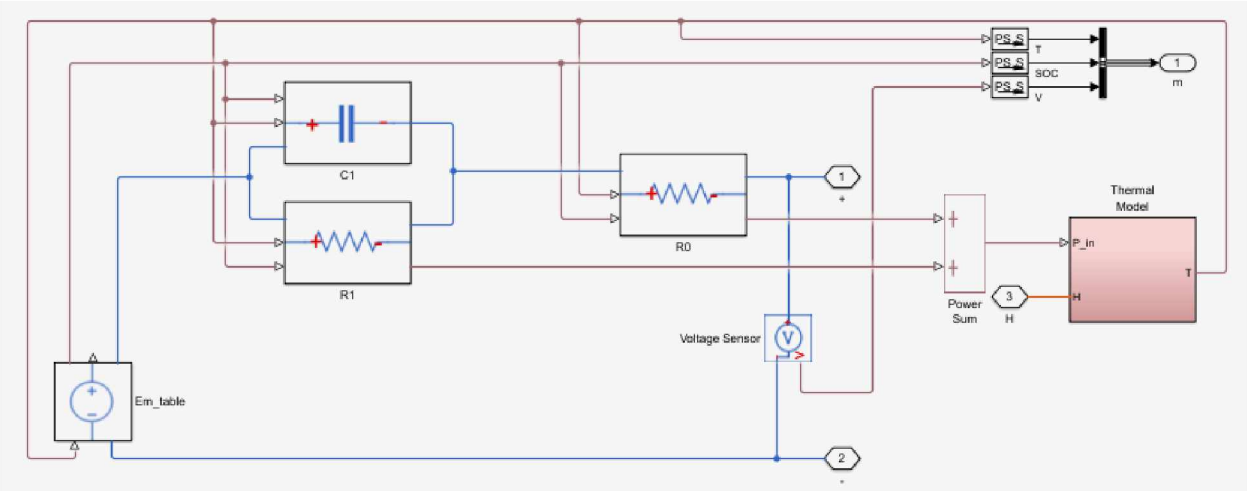

Figure 3-1: Lithium polymer single RC cell model [27].

As shown in Figure 3-1, the cell model is composed of four basic cell elements (R_0, R_1, C_1, and E_m), but also contains a thermal model. The thermal model is responsible for converting the power consumed by the internal resistances into heat, and then converting that heat into a temperature rise in the cell. Temperature rise is governed by five basic parameters; cell resistance values, current through the cell model, specific heat of the cell, mass of the cell, and the heat loss coefficient of the cell. The thermal model for this cell is given below in Figure 3-2.

This thermal model accepts a combined power sum from the loss components of the cell model (R_0 and R_1) as governed by (5) in Chapter 2. It also accepts ambient heat through convection, at the port labeled H in Figure 3-1. It then computes a cell temperature based on the specific heat of the cell and the total heat entering or leaving the cell, as given in (6) in Chapter 2.

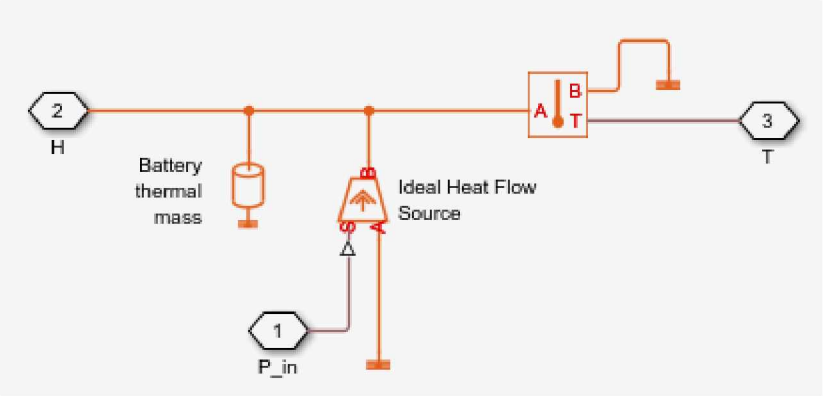

Figure 3-2: Thermal block of lithium polymer cell model. This models the thermal mass and converts power lost in the cell as heat energy into a cell temperature [27].

3.2 Measurement Methods and Errors

Throughout testing of the actual cells in the environmental chamber, the following methods were used to obtain values and take measurements.

The environmental chamber used in this research is an extreme environment chamber, manufactured by Associated Environmental Systems. It is capable of producing an internal temperature from -80 °C to 175 °C. It can maintain its set point with +/- 1 °C accuracy for tests lasting up to 2 days. For longer duration tests, on the order of 10 days or more, the temperature may vary as much as 6 °C (observed) from the set point, due to humidity frosting over the internal temperature sensor.

For voltage testing, measurements were taken at the external terminals of the cell, which gives a good representation of actual cell voltage. There is no way to directly measure E_m of the cell, since it is an abstract concept used to construct a working model of the cell and does not exist at a physically measureable point. The error in terminal voltage measurements is +/- 10 mV according to specifications of the testing equipment, West Mountain Radio CBA IV Pro. This is a computerized battery analyzer capable of supplying a load of up to 25 A continuous to the cell being tested. It is programmable using a simple interface and allows for constant current,

constant power, or constant resistance loads. In addition to constant loads, it can be configured for a duty cycle load, where the load, on-time duration, and off-time duration are all adjustable. More information on the CBA IV is given in section 4.1 (See Appendix A for manufacturer's technical specifications). Error induced in the voltage measurements by dissimilar metals (copper battery terminals ultrasonic welded to internal aluminum cell plates) was not investigated but is considered to be negligible.

Current measurements were taken using the CBA IV Pro. Accuracy is given as +/- 10 mA for currents less than 3 A and +/- 45 mA for currents between 3 A and 40 A. Testing indicated that the actual current measurement error was well within these specifications.

Temperature measurements were taken both with the CBA IV Pro (for cell temperature) and with an Omega 2176A digital thermometer (for ambient temperature). Ambient temperature was not logged for the duration of the test, as the Omega thermometer did not have logging capability, but was observed to remain steady within +/- 2 °C after settling. A temperature measurement precision specification is not listed for the CBA IV Pro, but signal noise was observed to be within +/- 0.1 °C. Absolute temperature values were checked against the Omega digital thermometer and agreed within 1 °C. Cell temperature was measured at the surface of the cell, with the sensing thermistor touching the cell surface and covered with a layer of felt insulation to limit the effect of ambient air on the reading. Ideally, temperature would have been measured internal to the cell, but this was not possible without destroying the cell.

3.3 Determining Model Component Values

To determine values for developing the LUTs, a set of real world tests was completed in an environmental testing chamber. Although the testing chamber is capable of rapid and extreme temperature changes, for these tests the temperature was held constant through each test. The lithium polymer battery used in the test is a 1.8 Ah TURNIGY Nano-Tech pack rated at 65 C - 130 C discharge, consisting of three cells in series. The test consisted of setting the chamber temperature to the desired test temperature, connecting the battery in the chamber, and then cold soaking the battery for a minimum of 2 hours to assure a uniform temperature throughout the cell. The load test consisted of a pulsed discharge load at constant power, designed to load the

battery at 2 C (3.6 A for a 1.8 Ah battery). Each pulse was timed to discharge 10% of the battery's rated capacity, and then the cell was allowed to return to its resting state for 15 minutes.

The pulse discharge test was designed to determine specific components of the cell model. During the off-state, the cell voltage will return to its resting OCV for that specific SOC. When the current pulse is initially applied, the terminal resistance of the cell can be determined directly by the (near) instantaneous drop in terminal voltage and by knowing the cell current at that point. The combined R_1 and C_1 values can then be determined by the curve at the base of the discharge pulse as shown in Figure 2-4 in Chapter 2. The following values were determined by analyzing data taken in the environmental chamber. This data represents a best-fit model as determined by using the MATLAB® Simulink® Design Optimization tool.

Each component of the cell model has not just one value, but a table of values, known as a look-up table, or LUT. An example of the LUTs that drive the model component parameters is given below in Table 3-1. In this LUT, cell voltages are arranged with each column representing a separate temperature. Lower temperatures are given in the left columns and higher temperatures in the right columns. Additionally, each row represents a separate SOC with 0 at the top in row 1 and 1 (or 100%) at the bottom in row 11. This LUT contains temperature values of -20, -10, -5, 2, 12, and 20 °C, and 0 to 1 SOC in 0.1 increments.

Table 3-1: Look-up table driving cell open-circuit voltage E_m. SOC ranges from 0 (top row) to 1 (bottom row) in increments of 0.1. Temperature breakpoints, from left to right, are -20 °C, -10 °C, -5 °C, 2 °C, 12 °C, and 20 °C.

E_m (V)						
SOC	-20 °C	-10 °C	-5 °C	2 °C	12 °C	20 °C
0.0	3.5000	3.5000	3.5000	3.5000	3.5000	3.5000
0.1	3.6500	3.6500	3.7178	3.7233	3.7122	3.6987
0.2	3.7000	3.7000	3.7517	3.7545	3.7480	3.7384
0.3	3.7500	3.7464	3.7795	3.7886	3.7851	3.7777
0.4	3.7800	3.7940	3.8053	3.8121	3.8134	3.8094
0.5	3.8000	3.8246	3.8377	3.8406	3.8401	3.8389
0.6	3.8500	3.8708	3.8863	3.8882	3.8899	3.8813
0.7	3.9000	3.9210	3.9245	3.9339	3.9363	3.9393
0.8	3.9500	3.9842	4.0194	4.0243	4.0326	4.0208
0.9	4.1000	4.1000	4.1314	4.1307	4.1306	4.1232
1.0	4.2000	4.2000	4.2000	4.1827	4.1848	4.1915

The three other LUTs used in this model, which drive R_0, R_1, and C_1 are derived at the same temperature and SOC breakpoints. The LUT in Table 3-2 is used to provide values for R_0 as a function of temperature and SOC. The LUT in Table 3-3 provides values for the R_1 block of the model. This, in conjunction with the C_1 block, determines the shape of rising and falling edges during pulse discharge events. The LUT in Table 3-4 provides values for the C_1 block of the model. This, in conjunction with the R_1 block, determines the shape of rising and falling edges during pulse discharge events.

Table 3-2: Look-up table driving cell R_0. SOC ranges from 0 (top row) to 1 (bottom row) in increments of 0.1. Temperature breakpoints, from left to right, are -20 °C, -10 °C, -5 °C, 2 °C, 12 °C, and 20 °C.

R_0 (Ω)						
SOC	-20 °C	-10 °C	-5 °C	2 °C	12 °C	20 °C
0.0	0.2600	0.3000	0.2000	0.0326	0.0248	0.0253
0.1	0.2600	0.0506	0.0291	0.0222	0.0121	0.0049
0.2	0.2600	0.1444	0.0297	0.0199	0.0118	0.0097
0.3	0.1300	0.0851	0.0312	0.0246	0.0158	0.0123
0.4	0.1300	0.0917	0.0316	0.0229	0.0139	0.0112
0.5	0.1300	0.0859	0.0309	0.0213	0.0122	0.0099
0.6	0.1300	0.0838	0.0315	0.0220	0.0127	0.0092
0.7	0.1300	0.0847	0.0308	0.0220	0.0127	0.0103
0.8	0.2500	0.0760	0.0309	0.0214	0.0138	0.0102
0.9	0.2000	0.1500	0.0250	0.0235	0.0148	0.0113
1.0	0.6700	0.2500	0.0160	0.0142	0.0055	0.0068

Table 3-3: Look-up table driving cell R_1. SOC ranges from 0 (top row) to 1 (bottom row) in increments of 0.1. Temperature breakpoints, from left to right, are -20 °C, -10 °C, -5 °C, 2 °C, 12 °C, and 20 °C.

R_1 (Ω)						
SOC	-20 °C	-10 °C	-5 °C	2 °C	12 °C	20 °C
0.0	2.0000	0.0038	0.0114	0.0260	0.0416	0.0492
0.1	0.7500	0.0080	0.0033	0.0033	0.0032	0.0032
0.2	0.2100	0.0202	0.0125	0.0139	0.0083	0.0059
0.3	0.1910	0.0151	0.0094	0.0138	0.0115	0.0102
0.4	0.1477	0.0140	0.0104	0.0140	0.0099	0.0075
0.5	0.1273	0.0149	0.0093	0.0113	0.0062	0.0054
0.6	0.1430	0.0148	0.0088	0.0109	0.0068	0.0060
0.7	0.1808	0.0148	0.0084	0.0114	0.0078	0.0070
0.8	0.1000	0.0151	0.0106	0.0159	0.0098	0.0089
0.9	0.2617	0.1500	0.0084	0.0123	0.0095	0.0098
1.0	0.8500	0.3000	0.0072	0.0076	0.0073	0.0064

Table 3-4: Look-up table driving cell C_1. SOC ranges from 0 (top row) to 1 (bottom row) in increments of 0.1. Temperature breakpoints, from left to right, are -10 °C, -5 °C, 2 °C, 12 °C, and 20 °C. Units in table are Farads.

C_1 (F)						
SOC	-20 °C	-10 °C	-5 °C	2 °C	12 °C	20 °C
0.0	400.0000	14.3490	0.8815	0.2627	0.1024	0.0037
0.1	500.0000	28719.3849	33414.9702	50759.8622	44541.6469	17860.0937
0.2	600.0000	1818.8581	2179.0286	3022.0604	3605.1918	3690.1375
0.3	846.0000	5832.3548	11289.1838	15720.7164	17987.6434	23726.4629
0.4	846.0000	8962.6666	7234.1581	8308.1235	10016.7663	11580.0311
0.5	846.0000	8772.7048	6226.4283	7180.5720	7239.5790	7240.4418
0.6	846.0000	8750.6877	5750.1800	6619.6848	6653.5441	6580.3366
0.7	846.0000	8565.8810	9030.2907	13150.9408	13000.8151	13314.8851
0.8	600.0000	7004.8065	3869.9321	4201.6622	3968.6694	3852.4591
0.9	846.0000	11188.4012	11851.0012	15103.1175	15707.2613	16920.3584
1.0	596.0000	7370.3258	7122.0298	6852.0356	7134.8917	7427.1758

As shown in Figure 3-3, the internal resistance of the cell, which is mostly determined by R_0, shows a very significant increase at temperatures below the freezing point, especially as the cell approaches zero SOC. Displaying the results graphically makes it easy to see what is happening as the cell undergoes extreme changes from a fully charged (SOC = 1) to a discharged (SOC = 0)

state across a 30 °C temperature range. The slight decrease in the value of R_0 at SOC = 1, -10 °C is most likely an artifact or error of the model, rather than an actual decrease. The most likely cause of error is due to the way the parameters are estimated and the way the discharge test is run. The test immediately starts at full discharge current, which does not allow any "settling" time of the initial value. This makes it very difficult for the optimization tool to make an accurate estimate of the parameter at time $t \leq 0$.

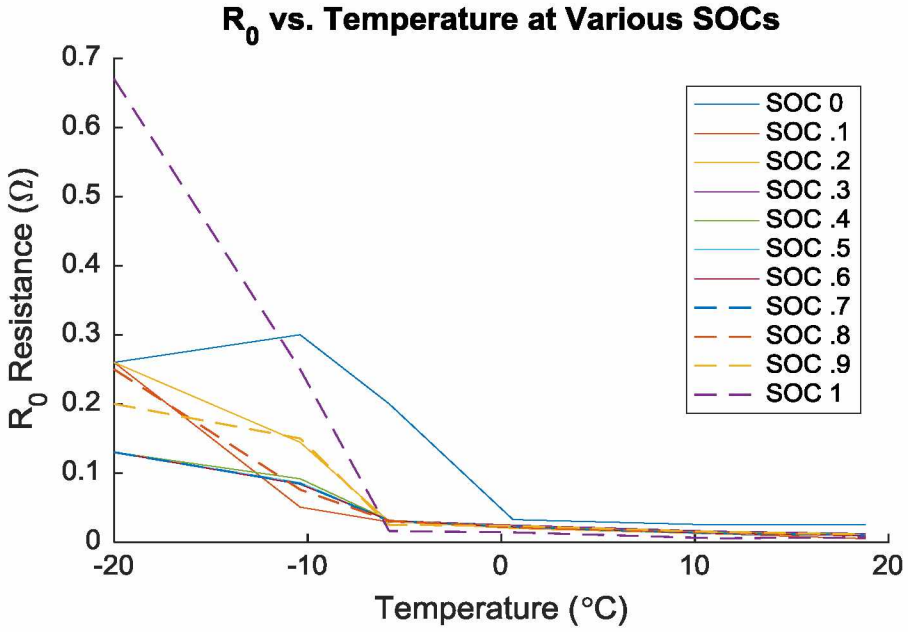

Figure 3-3: R_0 versus temperature at various SOCs.

Figure 3-4 shows how open circuit voltage of the cell is affected by temperature and SOC. As expected, for any given temperature, the open circuit voltage of the cell falls as the SOC decreases. The plot also illustrates that the voltage is not quite linear with SOC. As SOC decreases steadily, voltage initially falls off quickly and then nearly stabilizes until the pack reaches 0.1 SOC. It can also be seen that temperature does not have a huge effect on the open circuit voltage of the cell, when there is no load on the cell. However, the voltage will be greatly affected at low temperatures, especially below 0 °C, where there is a load on the cell, due to the increase in R_0.

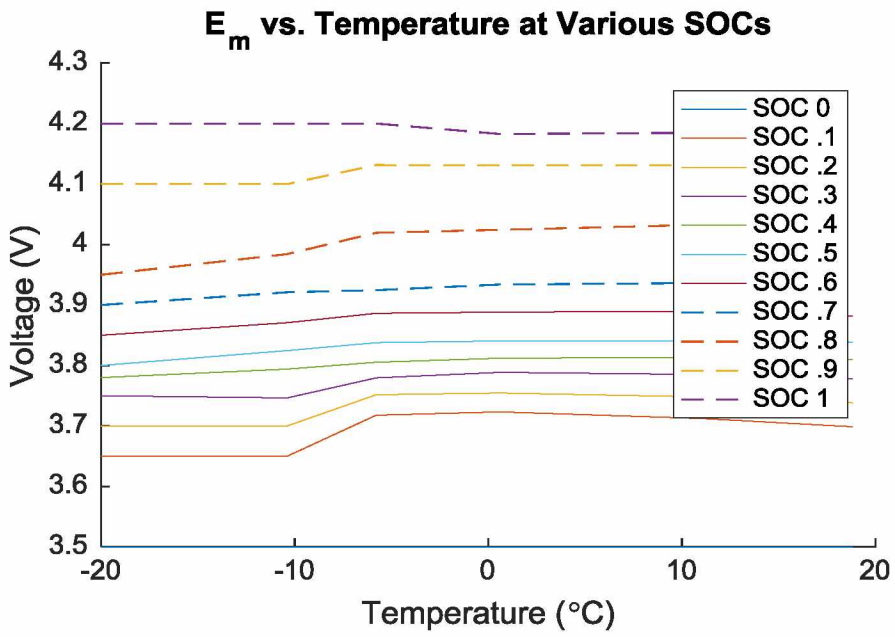

Figure 3-4: E_m versus temperature at various SOCs.

As shown in Figure 3-5, there is not a consistent correlation between R_1, temperature, and SOC. A general correlation can be made that as temperature decreases, R_1 increases, and this can be seen in the plot. At SOC = 0, totally discharged, R_1 values are outliers and do not appear to correspond to any known functions. This is not generally an issue with a cell model, however, as modeling a completely discharged cell is not often useful for real world applications. From the plots shown in Figure 3-6, it is not obvious what function the C_1 values correlate to. These are simply the best fits of the parameters R_1 and C_1 to the measured data.

In order to better understand the relationship of values of R_1 and C_1 to cell temperature and SOC better, they were combined together into a time constant, since that is what they are representing in the model. First, the values were multiplied element wise, and then the inverse value was taken by dividing a one's matrix by the element wise products of R_1 and C_1. Finally, the data row containing SOC = 0 was eliminated from the matrix because it resulted in values on the order of hundreds of seconds.

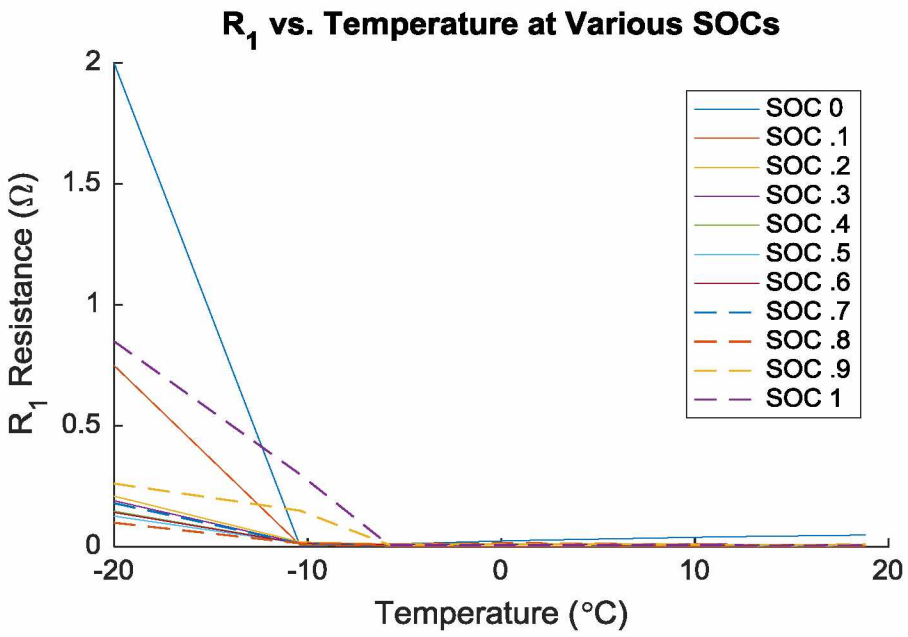

Figure 3-5: R_1 versus temperature at various SOCs.

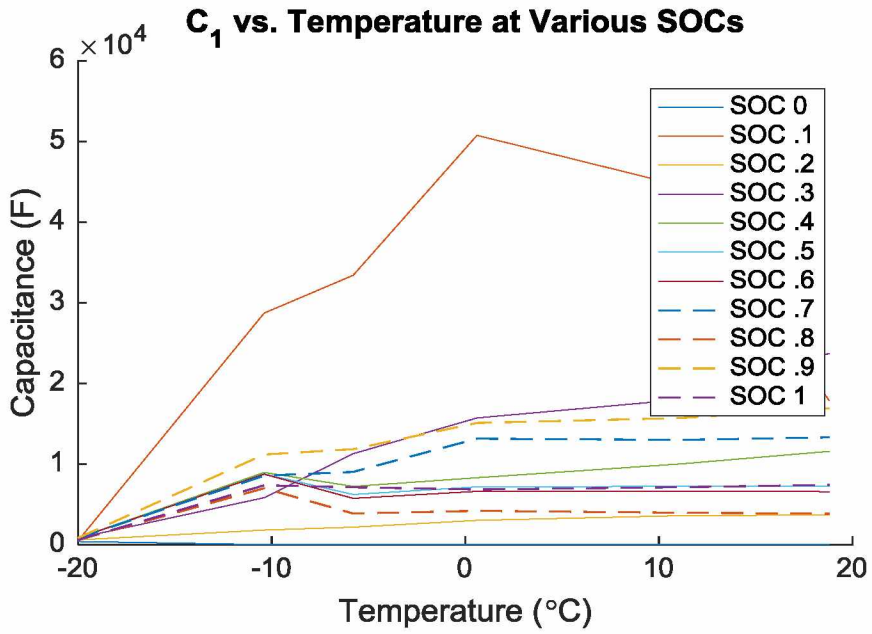

Figure 3-6: C_1 versus temperature at various SOCs.

As shown in Figure 3-7 below, the R_1C_1 time constant τ decreases as temperature decreases for the various values of SOC.

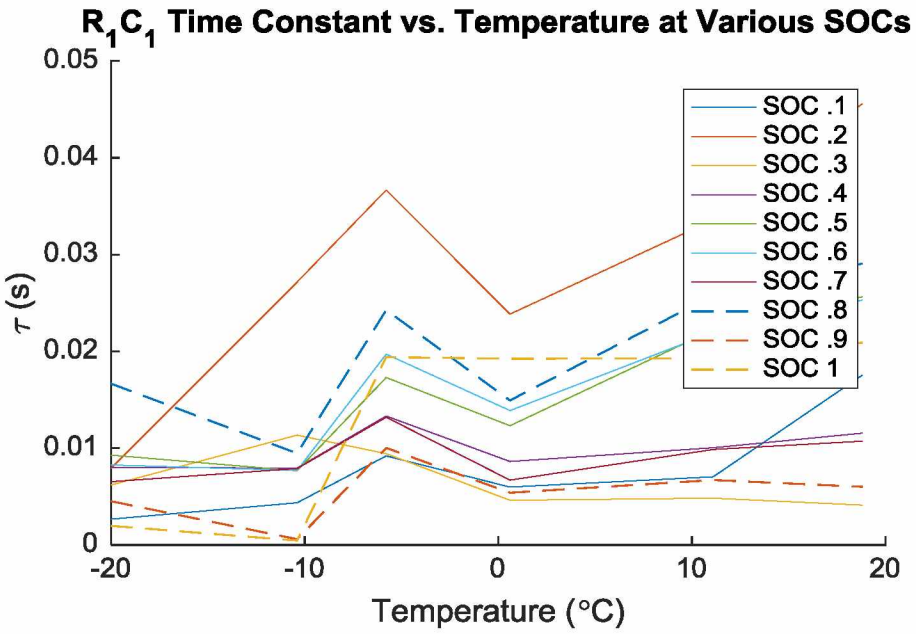

Figure 3-7: Time constant $\tau = R_1C_1$ versus temperature for various SOCs.

Now that the model topology has been chosen and values for the model parameters (R_0, R_1, C_1, and E_m) have been determined across a 40 °C temperature range from -20 °C to 20 °C at eleven SOC breakpoints, the model must be tested and validated. The results of model testing and validation, and the use of the validated model to simulate real-use scenarios of a battery powered all-electric snowmobile are presented in the following chapter.

Chapter 4: Results

In Chapter 3, the process of gathering data from cells at cold temperatures in the environmental chamber and then analyzing the measured results using MATLAB® Simulink® to optimize the $LiCoO_2$ model was discussed. In this chapter, the results and observations obtained from testing scenarios in the environmental chamber, validation of the battery model using the test data, and the use of the optimized $LiCoO_2$ model to simulate real-world scenarios are presented. This thesis places a heavy emphasis on the discharge parameters of the cell versus charging parameters for several reasons. Available equipment made it more difficult to gather accurate, highly detailed data during charging than during discharging. Discharging characteristics are generally more desired, as they are the characteristics that are most important when the battery is being used. In many charging scenarios the battery can simply be left on the charger for as long as necessary for a full charge and would often take place indoors in a heated area. Finally, the charge and discharge parameters of $LiCo0_2$ cells are very nearly equal, therefore, it would not provide much additional information to have LUTs for the charging cycle.

4.1 Model Optimization and Testing

Inside of Simulink® is a design optimization tool which helps optimize model component values so that model data will be a better fit to the measured data. An excellent feature of this toolbox is the ability to verify that the $LiCoO_2$ model matches the actual cell across a range of conditions. For example, two sets of discharge data can be collected at the same temperature, but with different discharge profiles. One set of data can be used to optimize model parameters so that the model output most closely matches the physical data. However, this would not necessarily mean that the model does a good job representing the actual cell, as it may perform differently if it is discharged under time varying conditions. In this case, the second set of data can be used to check how accurately the model and actual cell correlate with each other.

Because this verification tool did not easily lend itself to logging and storing data, the Simulink® model was modified with extra inputs and outputs. This allows environmental chamber data to be fed into the model with measured and simulated values being reported and stored.

Results of this thesis include data taken from the environmental chamber as well as simulated data generated by the tuned model. Environmental data was taken with a Computerized Battery Analyzer (CBA) built by West Mountain Radio. While somewhat limited in its capabilities, it is straight forward to use and has several very useful features. One of the most convenient features is the ability to perform a duty cycle (or pulse discharge) test on a cell or battery pack.

The pulse discharge test is configured and pre-loaded with cell capacity rating, nominal voltage, and minimum (cutoff) voltage. The type of pulse discharge test is selected, which can be constant current, constant power, or constant resistance. Test parameters are entered before the test is started. These include how much power (or current, or resistance) is drawn during each discharge pulse, how long each discharge pulse lasts, and the "resting time" between each of the discharge pulses. Resting time is important because it allows the cell to recover back to its resting voltage. This makes it possible to estimate the electrochemical voltage of the cell at each point. Figure 4-1 below shows a typical pulse discharge test setup.

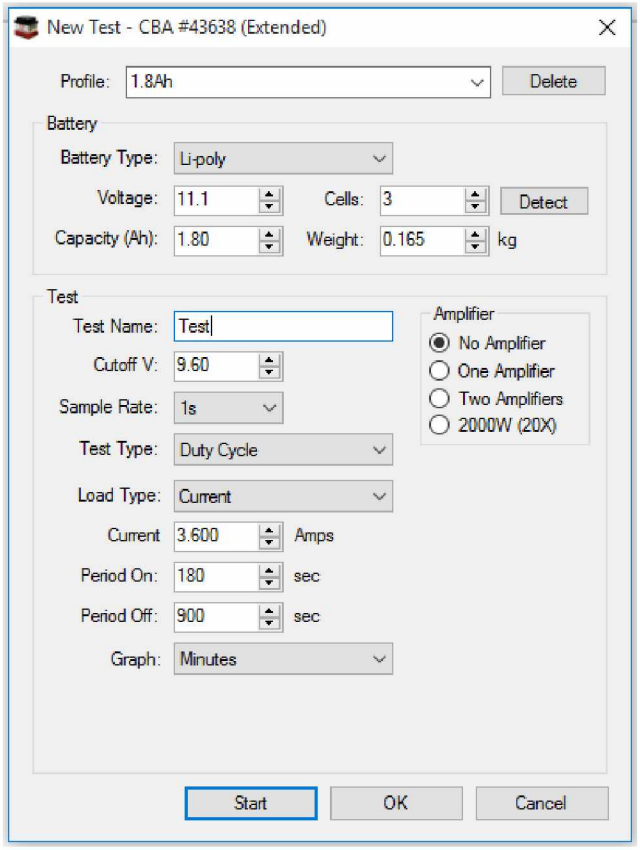

Figure 4-1: Discharge test setup page using West Mountain Radio CBA software.

In the following tests, a 1.8 Ah battery consisting of three cells connected in series was configured to fully discharge in 10 equally spaced pulses. The pulse lengths and magnitudes were configured to test the cells at ten distinct SOCs, in 0.1 increments from fully charged (SOC = 1) to fully discharged (SOC = 0). Initial tests were taken with constant-power discharge pulses of 50 W. Because of the series configuration of the set of three cells, this resulted in an initial cell current of 4 A, increasing to 5 A as the cell voltage decreased. At lower temperatures tests were performed with constant current discharge pulses, to avoid overloading the cell as voltage decreased. Figure 4-2 shows a plot taken at 20 °C to establish a baseline measurement for the cells to observe operation at a "typical" temperature.

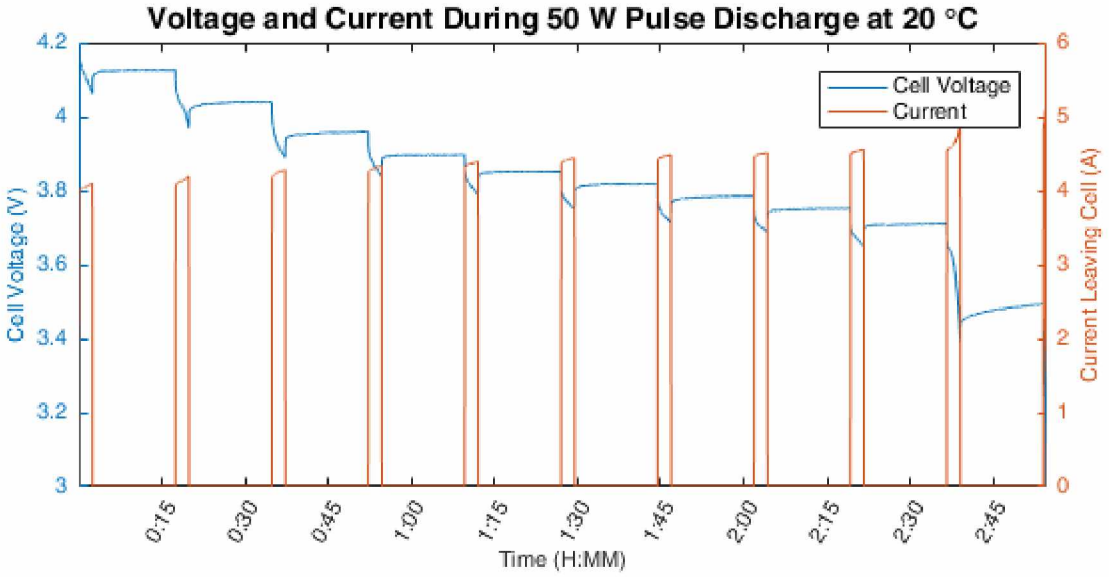

Figure 4-2: Plot of current and voltage during pulsed discharge test. Test is configured for constant power, causing current pulses to increase as voltage decreases. 50 W pulse is total across three cells. Data taken at 20 °C.

An interesting point to note in Figure 4-3 is that the voltage actually recovers to a slightly higher value at each interval than it does at the same point in Figure 4-2. However, the values are close enough that they are within the accuracy of the testing apparatus as discussed in Chapter 3 and serve to indicate that for temperatures above 10 °C, cell voltage and deliverable energy is largely unaffected by temperature.

Again, Figure 4-4 shows a very similar discharge profile, indicating that there is very little change across temperature range from 20 °C to 2 °C. Comparing Figure 4-4 and Figure 4-5, cell voltage cannot maintain the minimum 3.2 Vdc at -5 °C during the last discharge pulse between SOC = 0.1 and SOC = 0.

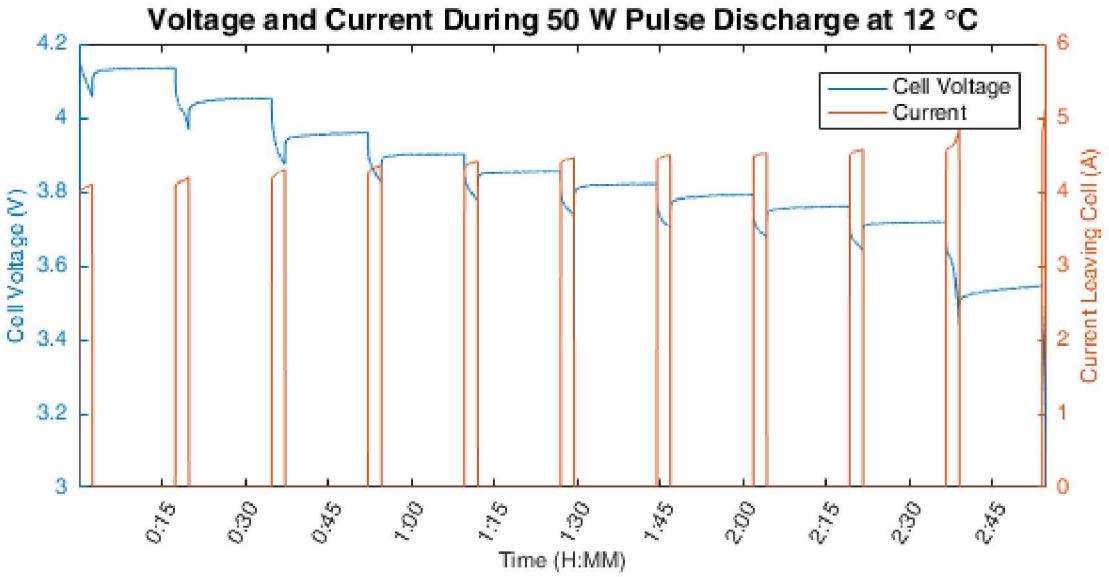

Figure 4-3: Plot of current and voltage during pulsed discharge test. Test is configured for constant power, causing current pulses to increase as voltage decreases. 50 W pulse is total across three cells. Data taken at 12 °C.

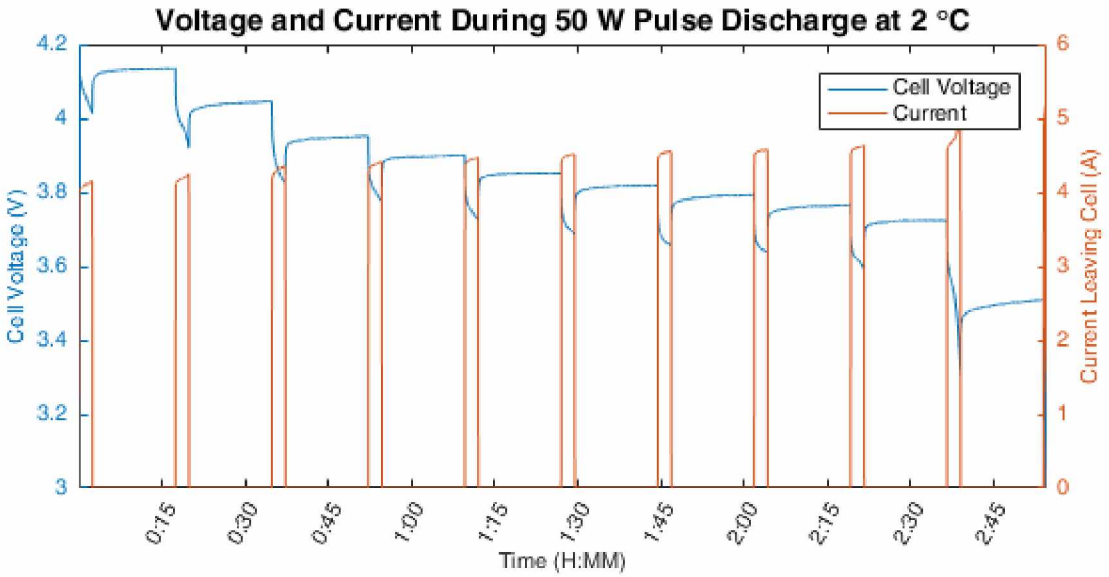

Figure 4-4: Plot of current and voltage during pulsed discharge test. Test is configured for constant power, causing current pulses to increase as voltage decreases. 50 W pulse is total across three cells. Data taken at 2 °C.

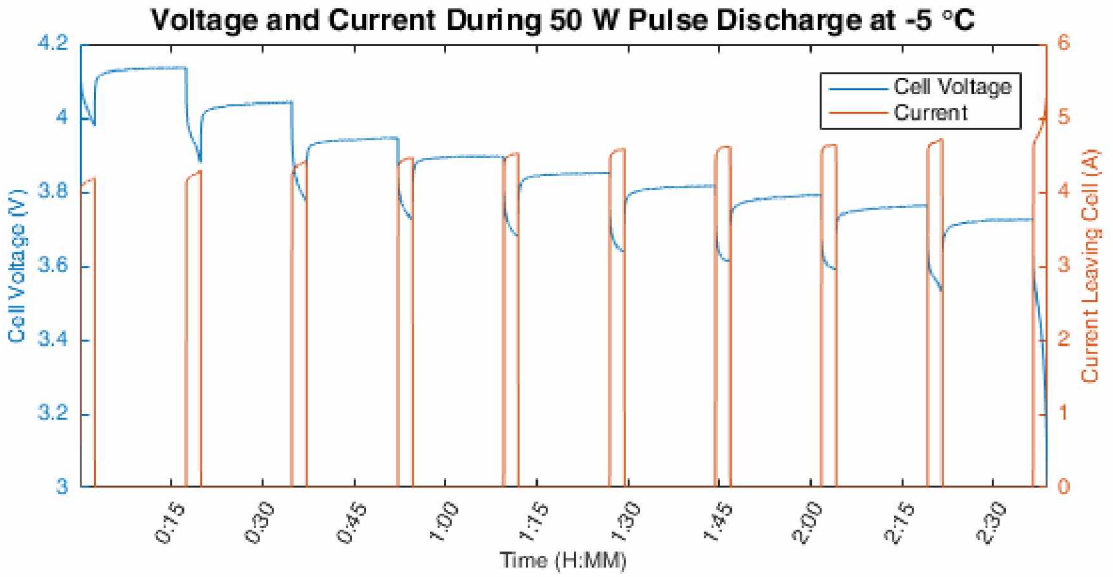

Figure 4-5: Plot of current and voltage during pulsed discharge test. Test is configured for constant power, causing current pulses to increase as voltage decreases. 50 W is total across 3 cells. Data taken at -5 °C.

In Figure 4-6, the testing parameters were modified for lower temperature, with a constant 1.8 A discharge pulse used instead of 50 W pulses. This is because the battery chemistry slows at low temperatures, making the cell incapable of providing as much current. Figure 4-7 shows a very similar profile at -15 °C as Figure 4-6 does at -10 °C, but overall voltage is slightly lower, and approaches the 3.5 Vdc level much sooner.

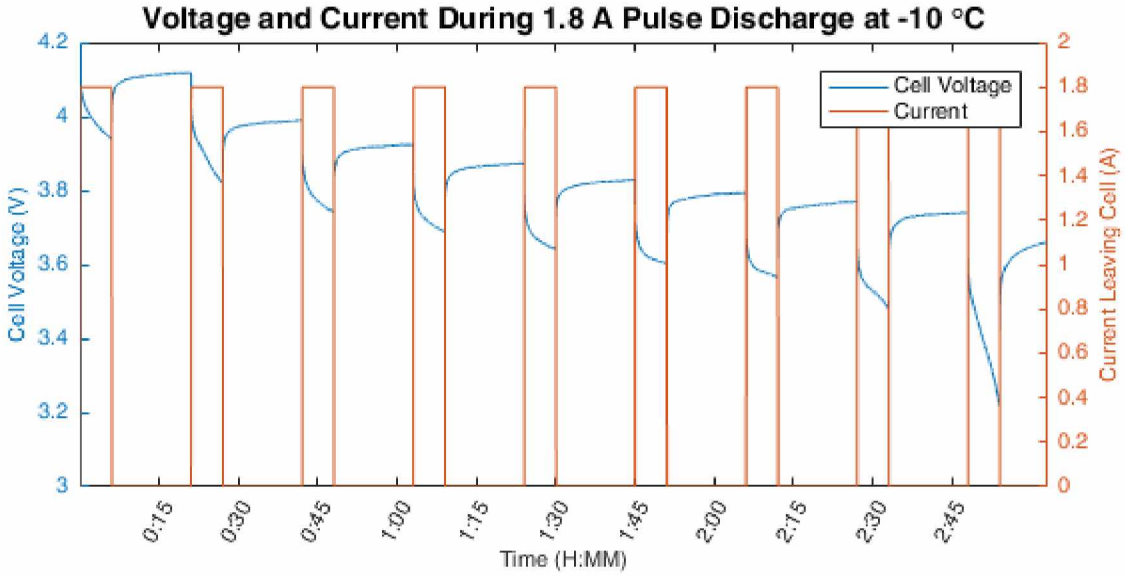

Figure 4-6: Plot of current and voltage during pulsed discharge test. Test is configured for constant current pulses of 1.8 A. Data taken at -10 °C.

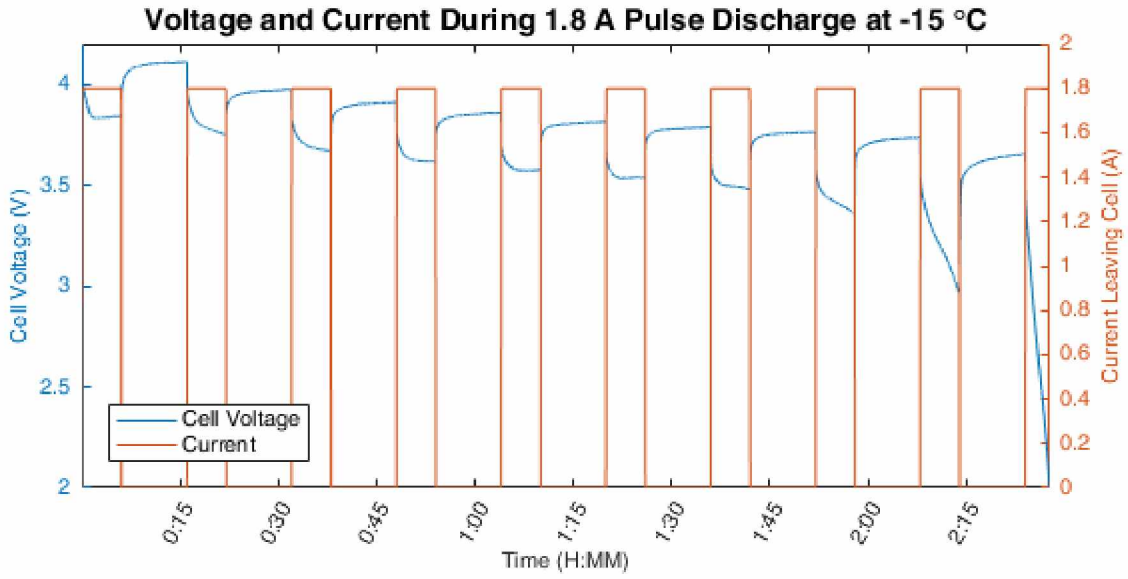

Figure 4-7: Plot of current and voltage during pulsed discharge test. Test is configured for constant current pulses of 1.8 A. Data taken at -15 °C.

The results of two tests that were configured to help keep the cell voltage from dropping too far while there was still energy remaining are shown in Figure 4-8 and Figure 4-9. The first of the two data plots shows current pulses of 1.8 A, while the second shows the current reduced by one half to 0.9 A. In warmer temperatures the cell could easily maintain these load levels, but at a temperature of -20 °C the effects of the cold on the cell performance are observed.

Figure 4-8 shows the dramatic effect that self-heating has on the cell, as the voltage initially dropped from 4.2 Vdc to just 3.3 Vdc, but then recovered to 3.7 Vdc while still under load. This is because the internal resistance of the cell causes it to warm from the inside, reducing internal resistance and increasing cell chemistry activity. This phenomenon is most prominent in low temperature and high current (load) conditions. In Figure 4-9, the current is reduced by one half to help minimize the effects of cell heating as well as decrease the extreme dips in voltage caused by IR losses. Here, the voltage does not dip and recover nearly as significantly as with higher currents. This is attributed to two different things. One, the lower currents causing less extreme voltage drops, and two, the internal heating is less severe and spread out over more time, so the cell has a longer time to lose heat to the environment. This keeps the internal cell temperature closer to ambient temperature.

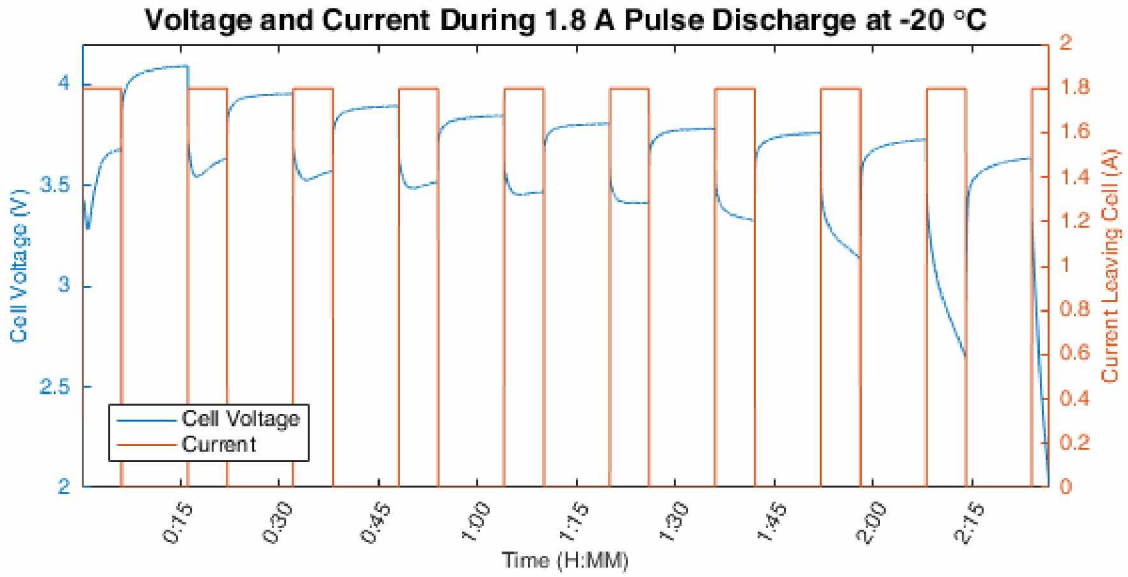

Figure 4-8: Plot of current and voltage during pulsed discharge test. Test is configured for constant current pulses of 1.8 A. Data taken at -20 °C.

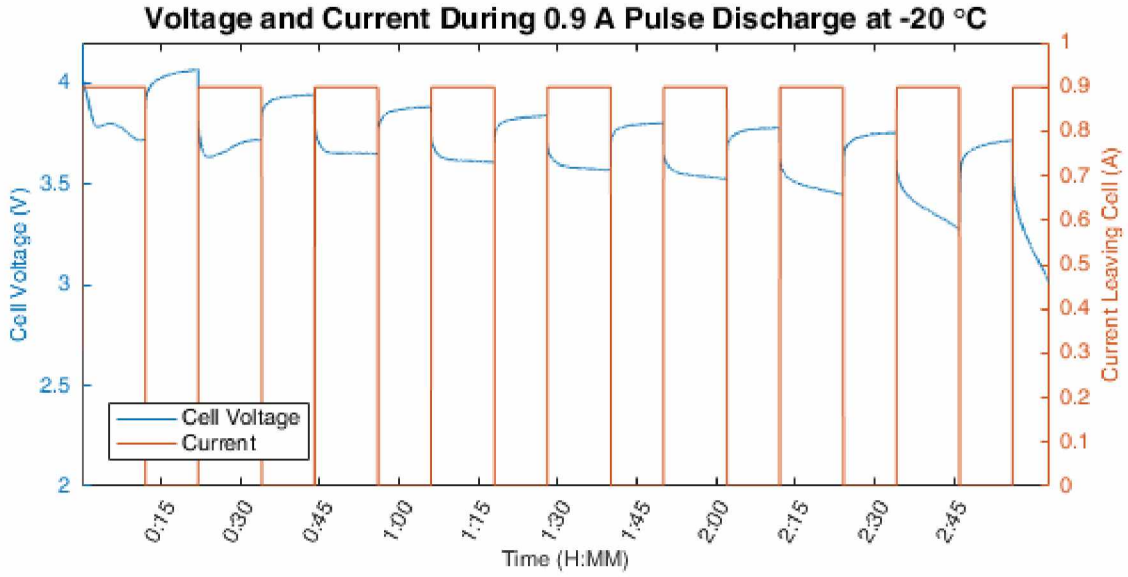

Figure 4-9: Plot of current and voltage during pulsed discharge test. Test is configured for constant current pulses of 0.9 A. Data taken at -20 °C.

Observations from the previous eight plots (Figures 4-2 through 4-9) indicate that there is a small effect on cell performance between 20 °C and 0 °C, and a much larger effect between 0 °C and -20 °C. There are several significant aspects of this effect which are worth noting. 1) The cells are able to supply nearly the same Ah capacity at low temperatures as warm temperatures. 2) The greatly increased internal resistance of the cell at low temperatures limits the useful energy that is extractable from the cell. 3) Increased resistance at low temperatures greatly limits

the peak power that can be drawn from the cell when it is cold. Finally, it is easy to see the effect that internal self-heating has on the cells, where the voltage initially dips when the cells are operated at low temperatures and then climbs to a value close to what it would be if the cell were operated in a warm ambient environment.

Throughout testing, it was seen that cell capacity (in Ah) is only very slightly affected by temperature, ranging from 1.8 Ah at 20 °C to 1.7 Ah at -20 °C. However, cell energy capacity (in Wh) is further diminished, as shown in Figure 4-10. Here, measured cell energy capacity exceeds the rated value by 3% at temperatures above 0 °C, but falls to 89% of rated capacity at -20 °C.

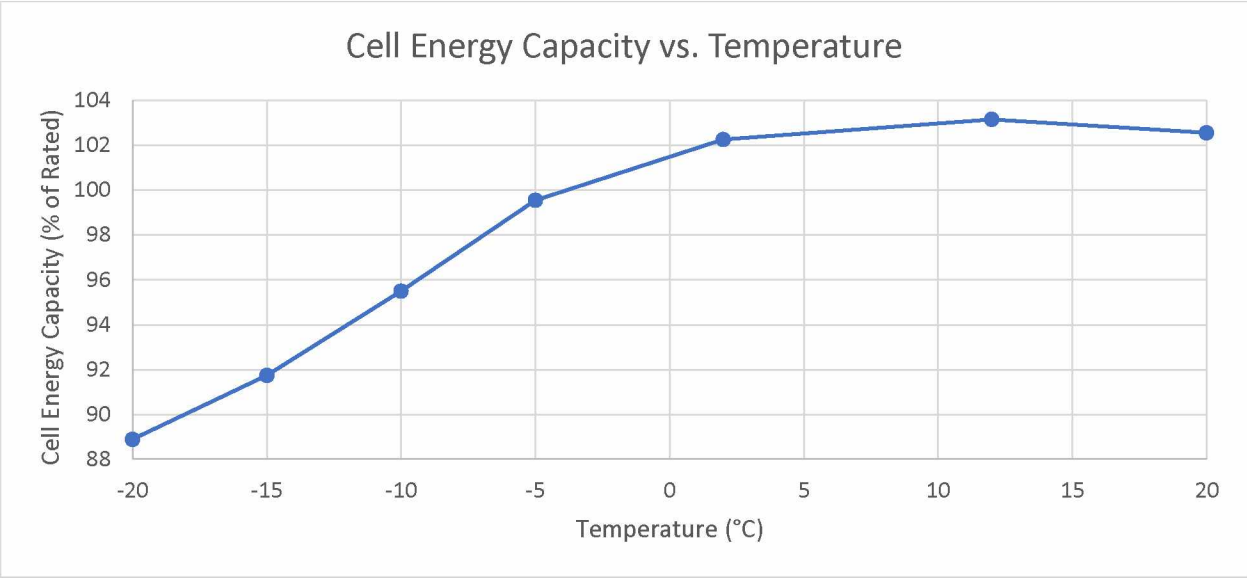

Figure 4-10: Cell energy capacity (Wh) as a percentage of rated cell energy capacity (%) across a 40 °C temperature range illustrating diminished cell performance at temperatures below -5 °C.

These results illustrate that the largest and most detrimental effect on the cells at low temperatures can be attributed almost entirely to increased internal resistance of the cell. The slightly lower value for Ahs extracted from the cell is mostly due to the cell reaching the pre-defined cut-off voltage earlier in the cycle, which is due to the increased voltage drop across the internal resistance of the cell. The lower energy delivered (in Wh) can also be attributed to increased internal resistance, as more of the total energy produced by the electrochemical activity of the cell is converted to heat before it can be used to do useful work. These results indicate that if a battery pack is appropriately sized (big enough), so that the load current per cell is limited to a small value during use rather than operated at the upper end of the manufacturer suggested

range, the battery pack will be able to perform acceptably across the entire temperature from -20 °C to 20 °C.

4.2 Validated Model

Figure 4-11 shows the completed MATLAB® Simulink® model used to validate cell parameter values (R_0, R_1, C_1, and E_m) calculated with the MATLAB® Simulink® Design Optimization tool as originally developed in [27]. As configured, the model accepts measured cell temperature, current, and voltage. These values were all logged in the environmental chamber and compiled into data tables, which are then displayed on the model scopes as measured data.

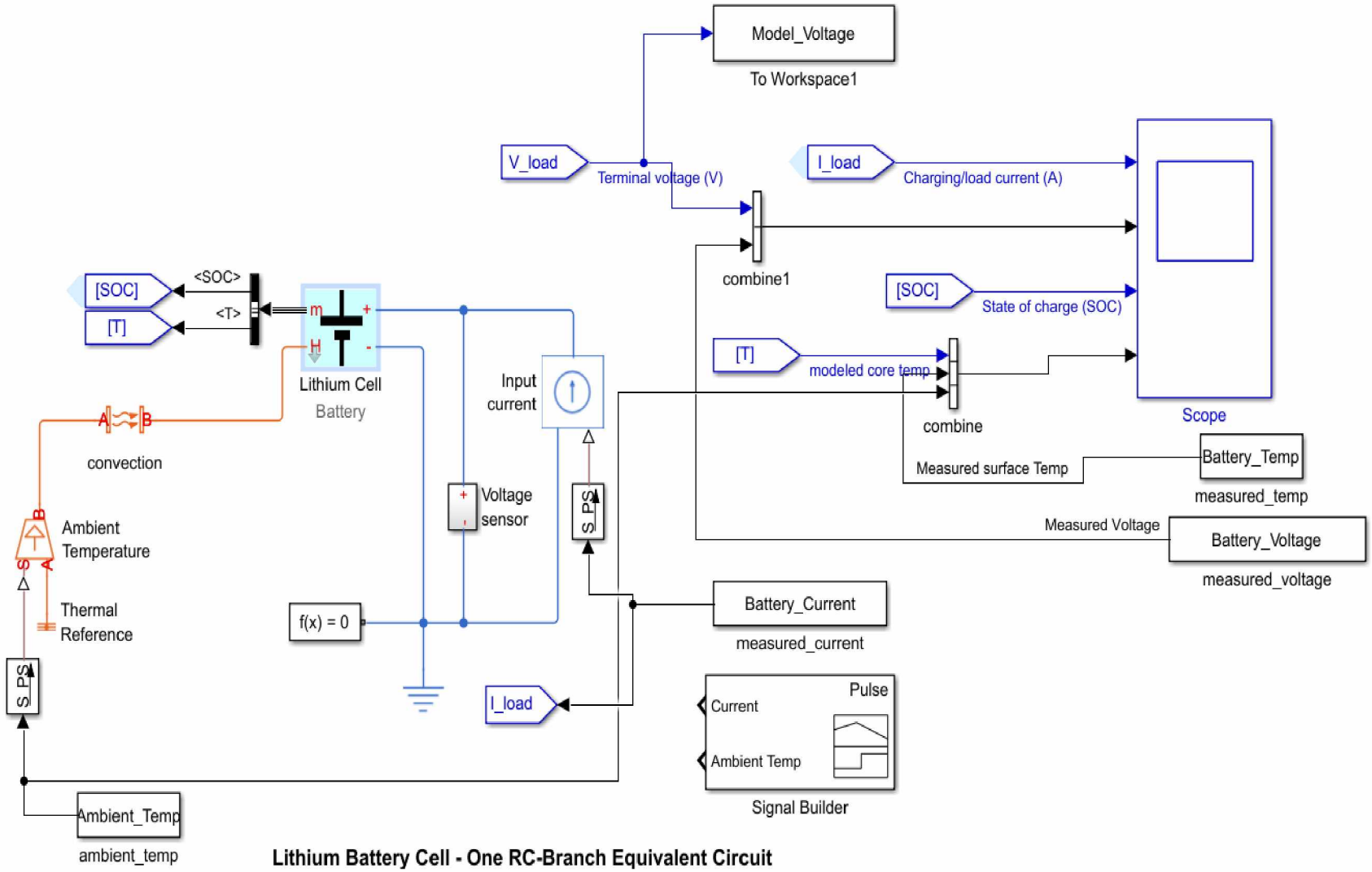

Figure 4-11: Simulink model used to validate cell parameters [27].

In testing, an issue was found with the model when discharging cells at very low temperatures. The optimization routine is designed around an isothermal cell discharge test. As configured, the model expects a decaying exponential voltage response that mimics an RC circuit, with a capacitor being either charged or discharged through a resistor. This gives a response resembling Figure 4-9 from 1:00 to 2:15 (H:MM). Here, the voltage approaches one of two values, depending on if the cell is open circuited, or being discharged. When open circuited, the terminal voltage approaches a steady state DC value equal to E_m, the electrochemical voltage produced internally in the cell. During discharge, the terminal voltage approaches the value given by (7).

$$V_{terminal}=E_{m(SOC)} - (I_{cell})(R_0+R_1) \tag{7}$$

Here, $V_{terminal}$ is the voltage seen at the terminal of the cell, $E_{m(SOC)}$ is the electrochemical voltage produced by the cell and is a function of SOC, I_{cell} is the cell current, and R_0 and R_1 are the internal resistance components of the cell.

As seen during the first 5 minutes of discharge in Figure 4-8, the voltage response at low temperatures and relatively high current values looks very different from a decaying exponential. This is because in these conditions the cell is non-isothermal. The cell initially starts discharging when cold, and the current through the resistance of the cell rapidly increases the temperature. For a given current value, decreased internal resistance causes a rise in terminal voltage. This effect is caused by internal heating of the cell decreasing the internal resistance. This effect is amplified at lower temperatures due to the exponential increase in resistance for an incremental decrease in ambient temperature.

One way to mitigate this issue is to simply discharge the cell slower. If the test is run slowly enough, the cell loses heat faster than it creates it. The primary drawback of this is how long it takes to collect data. At the very bottom of the usable temperature range, these cells exhibit an internal resistance on the order of several ohms per cell for a 1.8 Ah pack. This necessitates a discharge rate of around C/20, or a full 24 hours for a single discharge cycle. Since cell parameters (especially internal resistance R_1 and R_0, but also C_1 to a lesser extent) can vary with small changes in temperature, it is desirable to have data points at increments of 5 °C. Because of this, it would take several weeks to fully map the parameters of a single cell at low temperatures using this method.

To take data more expediently, and to get a better idea of how the cells will operate at rated capacity rather than a much-reduced rate, data was taken near a 1 C rate. To get around the limitations of the model, parameters were estimated for a given temperature and used as initial guesses. Data was then taken at a lower temperature, and used to correct the previous values. The validation model accounts for temperature rise in the cell, and can accurately plot voltage response as the cell temperature changes during discharge.

The model injects measured ambient temperature and measured cell current to the combined thermal block and configured temperature-specific LUTs to calculate an appropriate voltage response and cell temperature rise. In Figure 4-12 and Figure 4-13, the current, modeled and measured voltage, % error between modeled and measured voltage values, SOC, and modeled, measured, and ambient temperatures (averaging -6 °C and -10.3 °C, respectively) are plotted as a function of time. These plots illustrate the correlation between measured and modeled cell values.

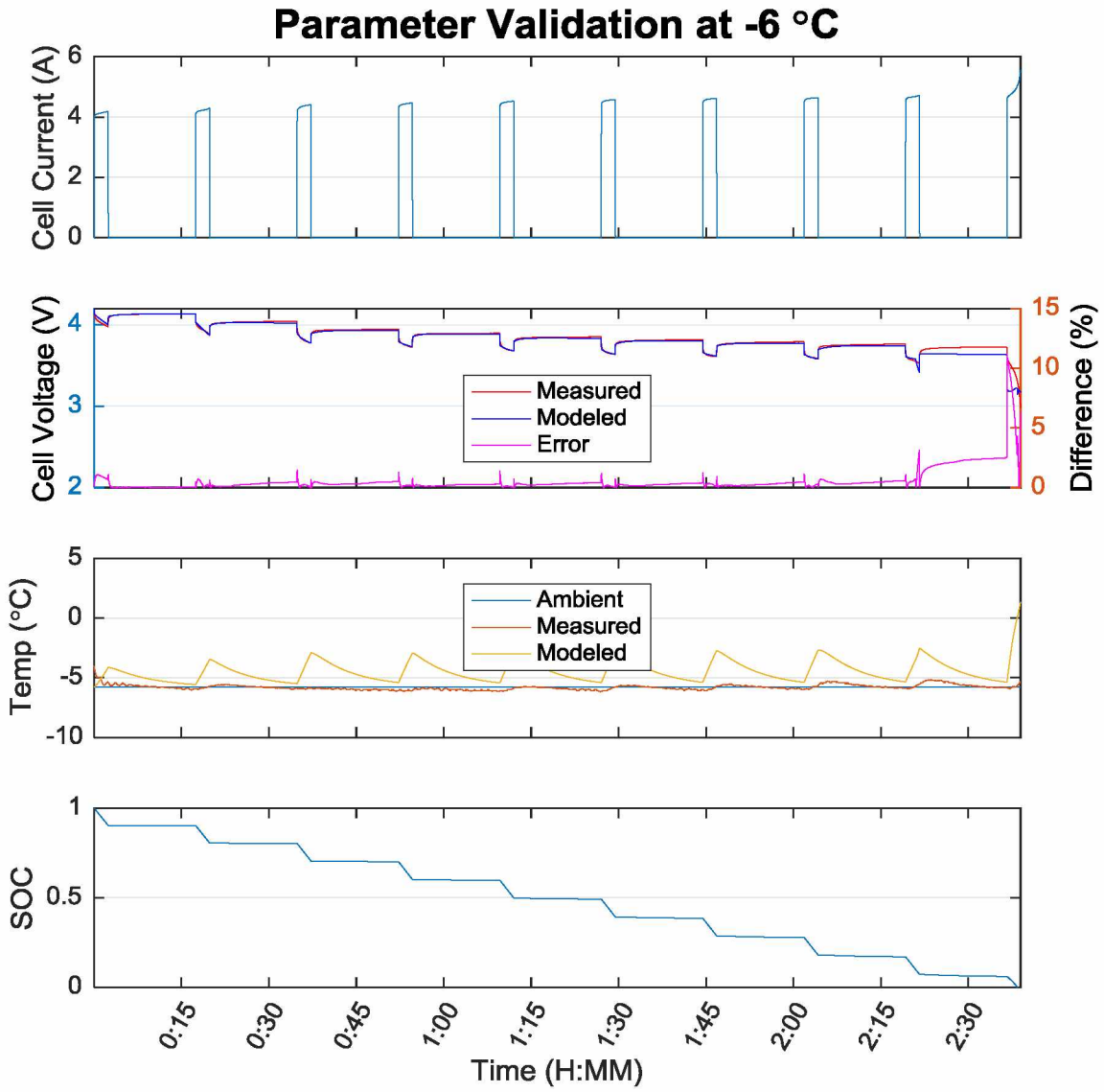

Figure 4-12: Modeled and measured cell voltage response to a 16.67 W/cell discharge pulse at ambient temperature of -6 °C.

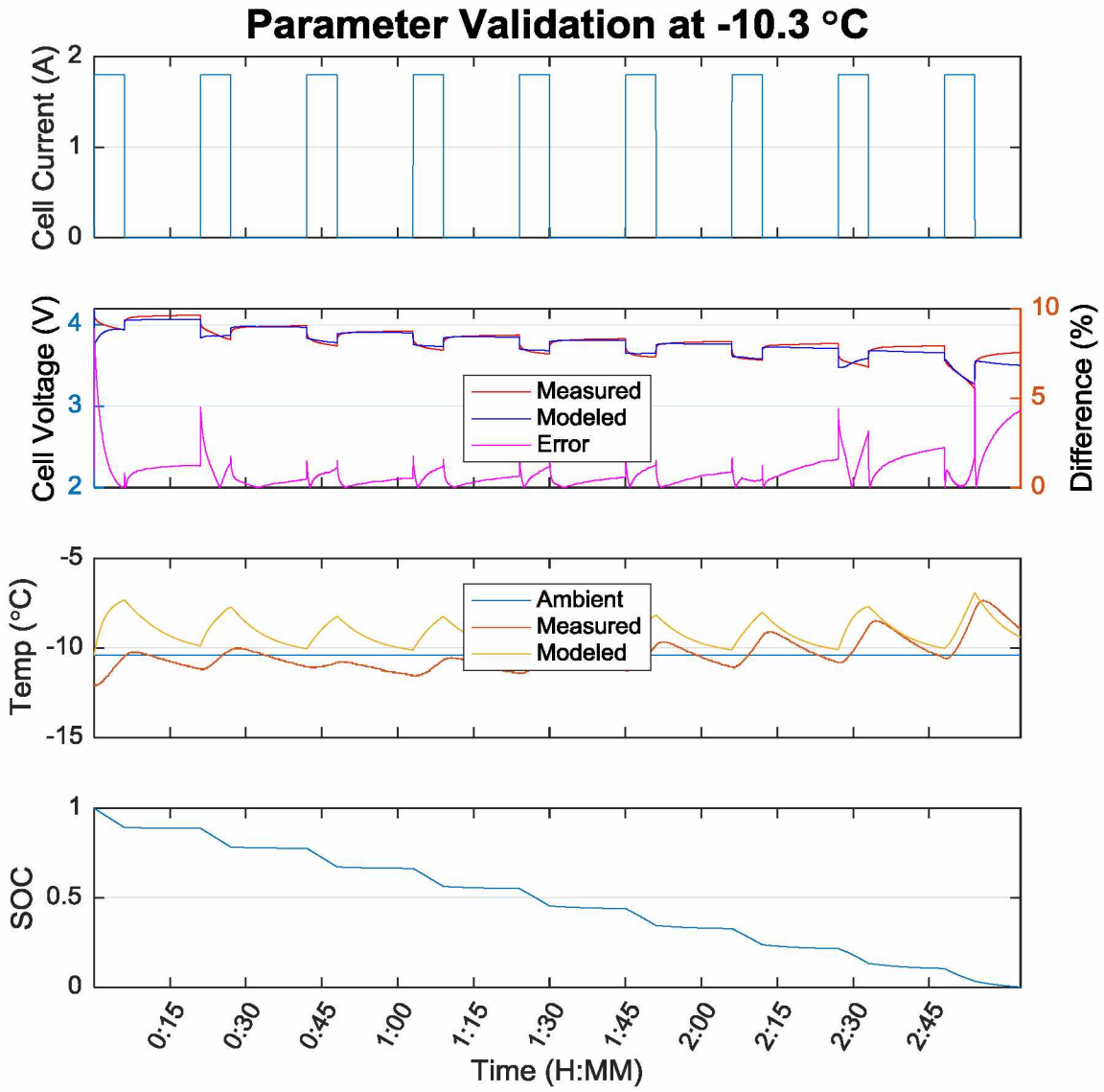

Figure 4-13: Modeled and measured cell voltage response to a 1.8 A discharge pulse at ambient temperature of -10.3 °C. Modeled response matches measured response across the mid-range of SOC, which is where the cell would normally be operated.

In Figure 4-14, the effect of self-heating is easily seen. The cell initially starts at -20 °C and then rapidly heats to -12.5 °C within the first discharge pulse. The effect on voltage is seen in the voltage subplot, where the cell voltage increases under sustained discharge rather than decreasing. The model mimics this effect by shifting component values from the high-resistance values in the -20 °C LUT column to the lower-resistance values in the -10 °C LUT column. Decreased internal resistance causes a higher terminal voltage for a given current value because less voltage is dropped across the internal cell resistance.

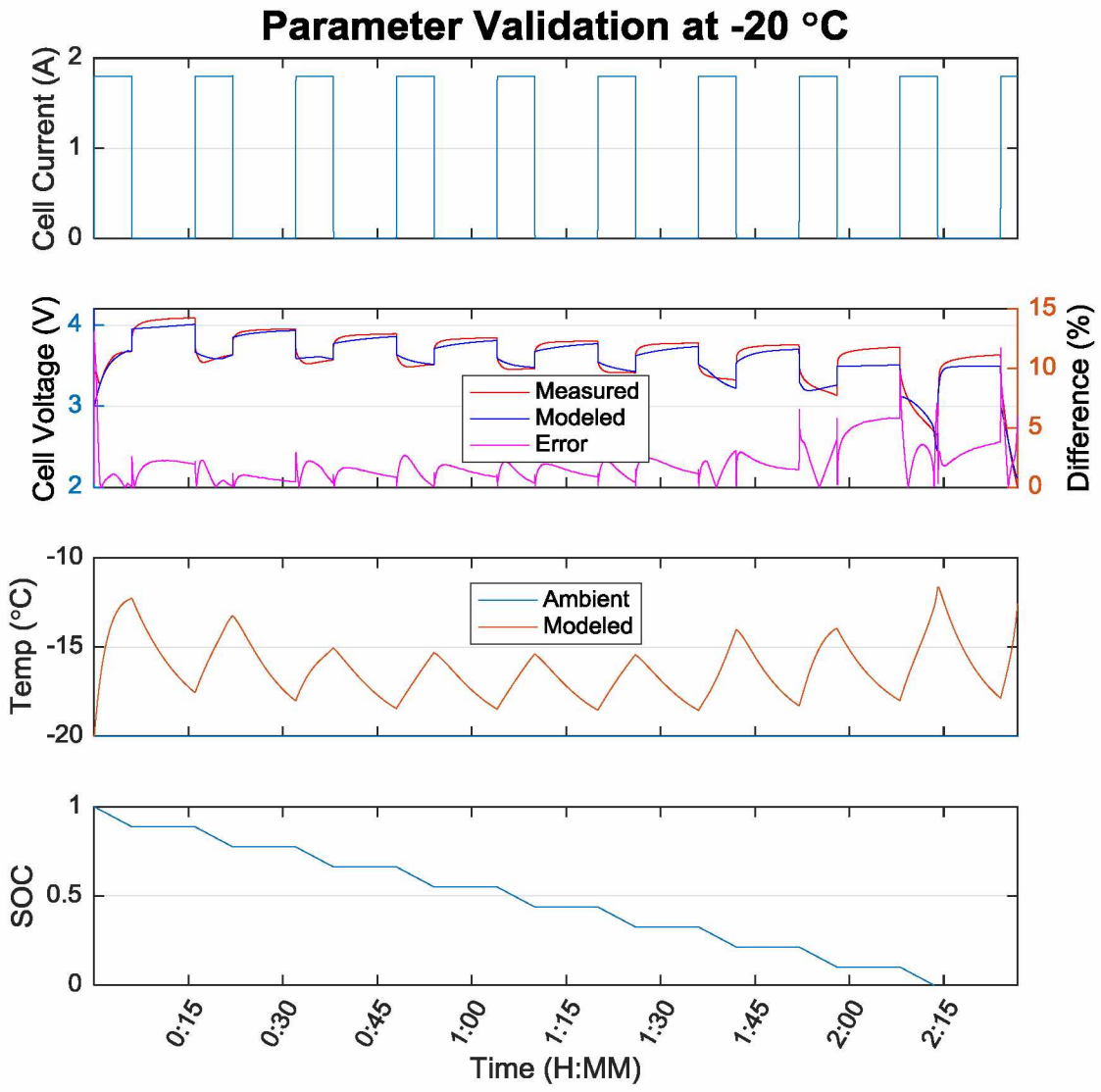

Figure 4-14: Modeled voltages closely match measured voltages in this pulse discharge plot. Data taken at ambient temperature of -20 °C and 1.8 A current pulses.

As a means of checking the accuracy of the model against measured results, a statistical analysis was performed between the voltage profile generated by the model, and the voltage profile measured in the environmental chamber. To look at the error, the measured and modeled results were compared at three temperature points, 20 °C, 2 °C, and -20 °C. Additionally, the discharge profile was split into three sections, the first section depicted the first 20% of discharge from SOC = 1 to SOC = 0.8, the second section depicted 60 % of discharge from SOC = 0.8 to SOC = 0.2, and the final section depicted the last 20% of discharge from SOC = 0.2 to SOC = 0.

These mean-squared errors in the cell voltage for the three part discharge profile are shown below in Table 4-1. Overall, the model results compare well with the measured results. The mean-squared error is lower for warmer temperatures and for the middle of the discharge profile. The highest mean-square error is at -20 °C for SOC < 0.2 (near the point of full discharge) and corresponds to an error of 138 mV.

Table 4-1: Calculated mean-squared error between measured and modeled cell voltages. Errors calculated at three distinct temperatures and three SOC ranges.

Mean-Squared Error (V^2) vs. Temperature (°C)			
	SOC > 0.8	0.8 > SOC > 0.2	SOC < 0.2
20 °C	0.0000142	0.0000071	0.0026081
2 °C	0.0000262	0.0000344	0.0004778
-20 °C	0.0067265	0.0034225	0.0190554

4.3 Energy Scenario Testing

Finally, a "real use" case scenario was set up, where the battery is subjected to conditions that might be encountered in the real world. In this scenario the battery, installed in a snowmobile, starts in a garage at an elevation 255 m above sea level. The machine leaves a garage kept at 20 °C and drives outside, where the ambient temperature is -10 °C. The machine is then driven down to the Chena River, elevation 128 m above sea level, where the ambient air temp is -20 °C. After a short drive on the river, the machine drives back up the hill and re-enters the garage.

Figure 4-15 shows the results of this scenario test using a 1.8 Ah cell discharged in the environmental chamber. Data was collected and plotted, and then processed using the model and compared to measured results. The model does a reasonable job of calculating cell response and matching modeled values to measured values. In the first plot window, cell current is shown. The model is configured so that negative current values are representative of current leaving the cell.

While current increases in each step, the temperature also changes at each point. This simulates the battery experiencing changing environmental conditions, such as the outside ambient temperature dropping. Specifically, this test is designed around the idea of temperature dropping as elevation decreases. This is also why cell current increases dramatically at the end of the test, as the machine being powered by the battery is assumed to climb back up the hill to return to the garage it started in. Initially, the cell starts at a very light load of only 1 A, then is increased in steps up to a maximum of 4 A before returning to its initial value of 1 A, and is then disconnected completely.

Using the validated cell model, several other scenarios were tested to examine the effects of storing the battery inside versus outside, and the effect of insulating the battery pack versus leaving it open to the atmosphere. All four of the following tests were conducted at an ambient temperature of -10 °C, using the same current profile. The baseline test was conducted with the initial cell temperature set to ambient temperature, simulating the battery being stored outside, and with no insulation added to the cell model. This is shown in Figure 4-16. Here, the cell voltage initially dips to just below 3.5 Vdc and then increases to 3.7 Vdc as cell temperature increases under load. The load is then removed and the battery is allowed to sit for one hour,

while it loses heat to the atmosphere. At this point, the load is re-applied and remains until the cell's energy is depleted. Total energy delivered during this test was calculated to be 5.14 Wh.

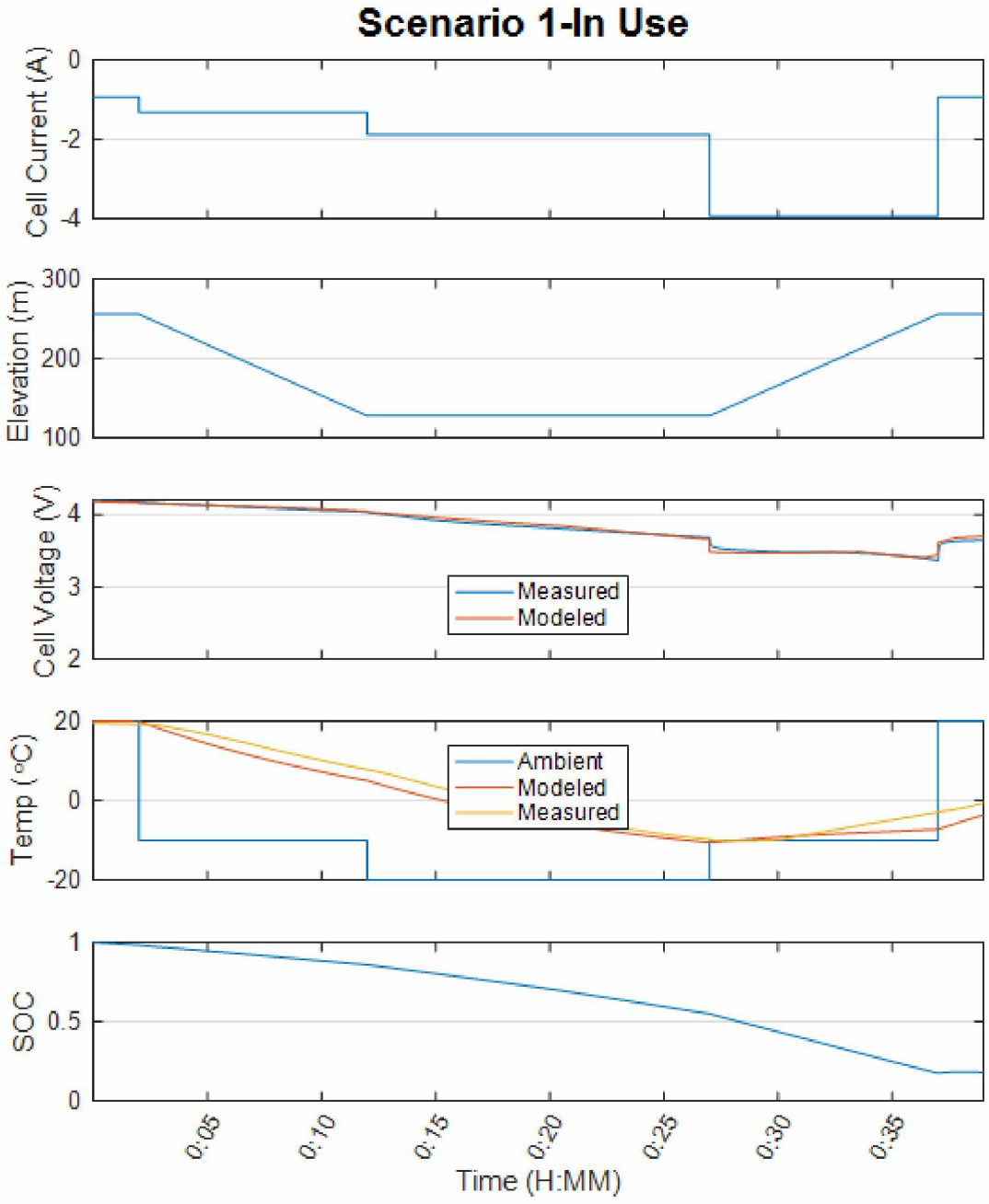

Figure 4-15: Measured and modeled cell response in a real-world usage scenario. Temperature during the discharge scenario ranged from 20 °C down to -10 °C.

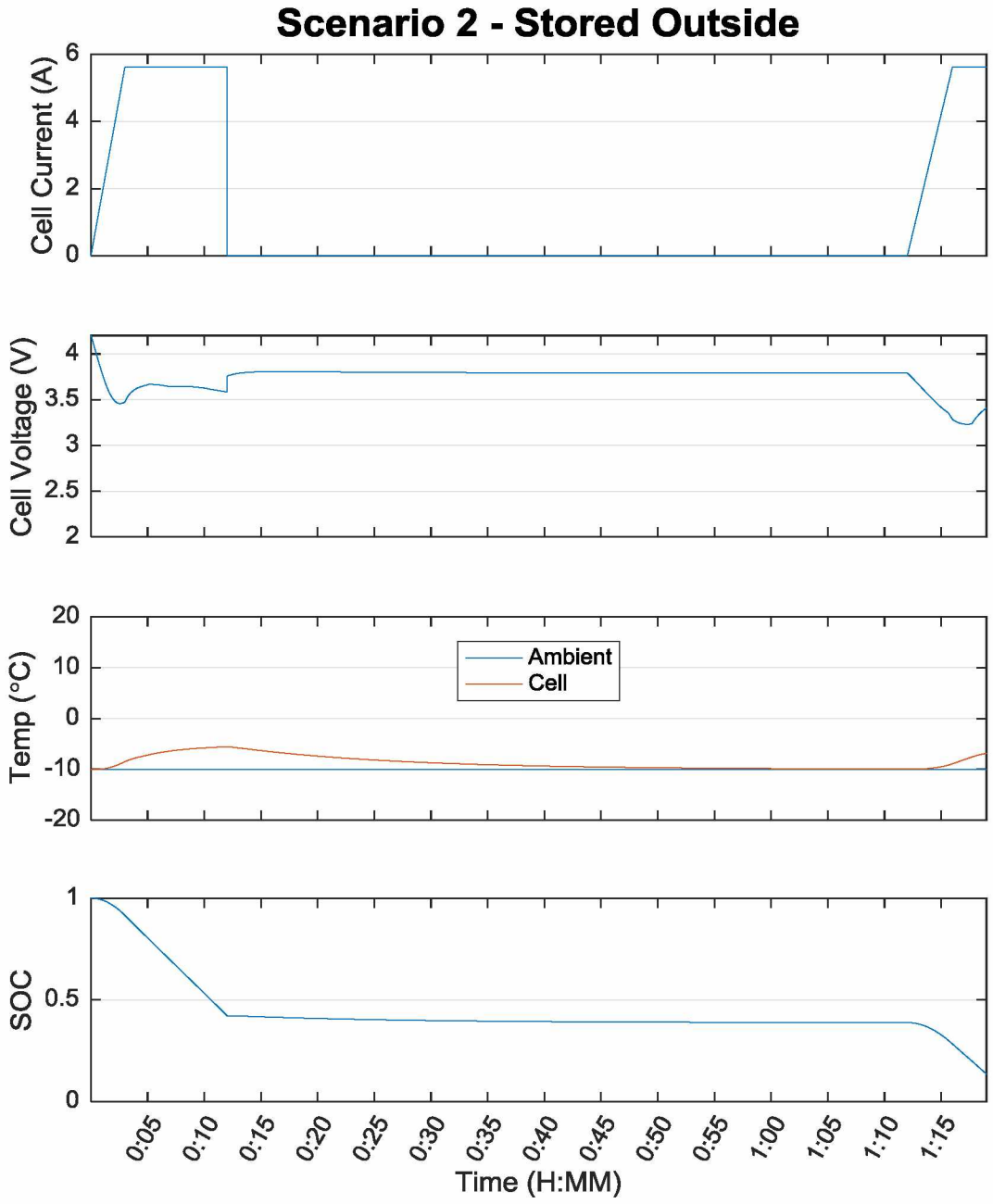

Figure 4-16: Baseline model-based scenario. Initial battery temp was set to ambient temp. Cell voltage and temperature were monitored as discharge current was applied. Total energy delivered was calculated to be 5.14 Wh.

After a baseline test was established, the effect of starting with a warm battery was explored. In Figure 4-17, it can be seen that the cell voltage does not show the same initial dip as it did when the battery started cold. During this phase, there was much more power available from the battery, and the final energy delivered was 5.38 Wh, versus 5.14 Wh with a cold start.

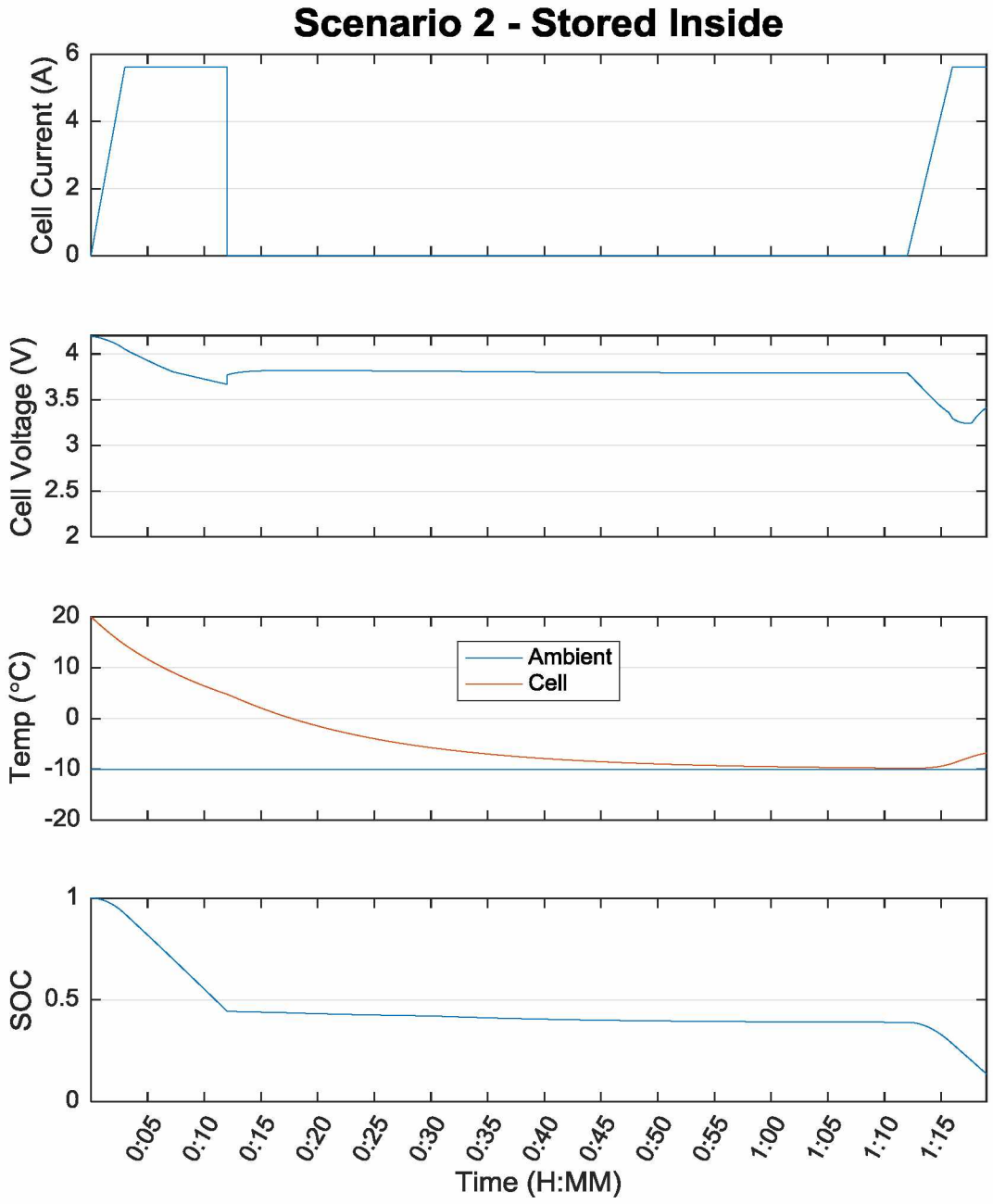

Figure 4-17: Model-based scenario simulating battery pack being stored inside warm garage. Initial battery temp was set to 20 °C. Cell voltage and temperature were monitored as discharge current was applied. Total energy delivered was calculated to be 5.38 Wh.

Next, the effect of insulation on a cold battery was explored. Figure 4-18 shows the effect of 5 cm (2 inches) of foam insulation, with the battery again stored outside at an ambient temperature of -10 °C. Cell voltage makes a sharp dip during the first discharge period, but this time there is no dip during the second discharge period. The cell maintains most of the heat

generated during the first discharge pulse. Energy delivered was 5.27 Wh, versus 5.14 Wh for a non-insulated battery.

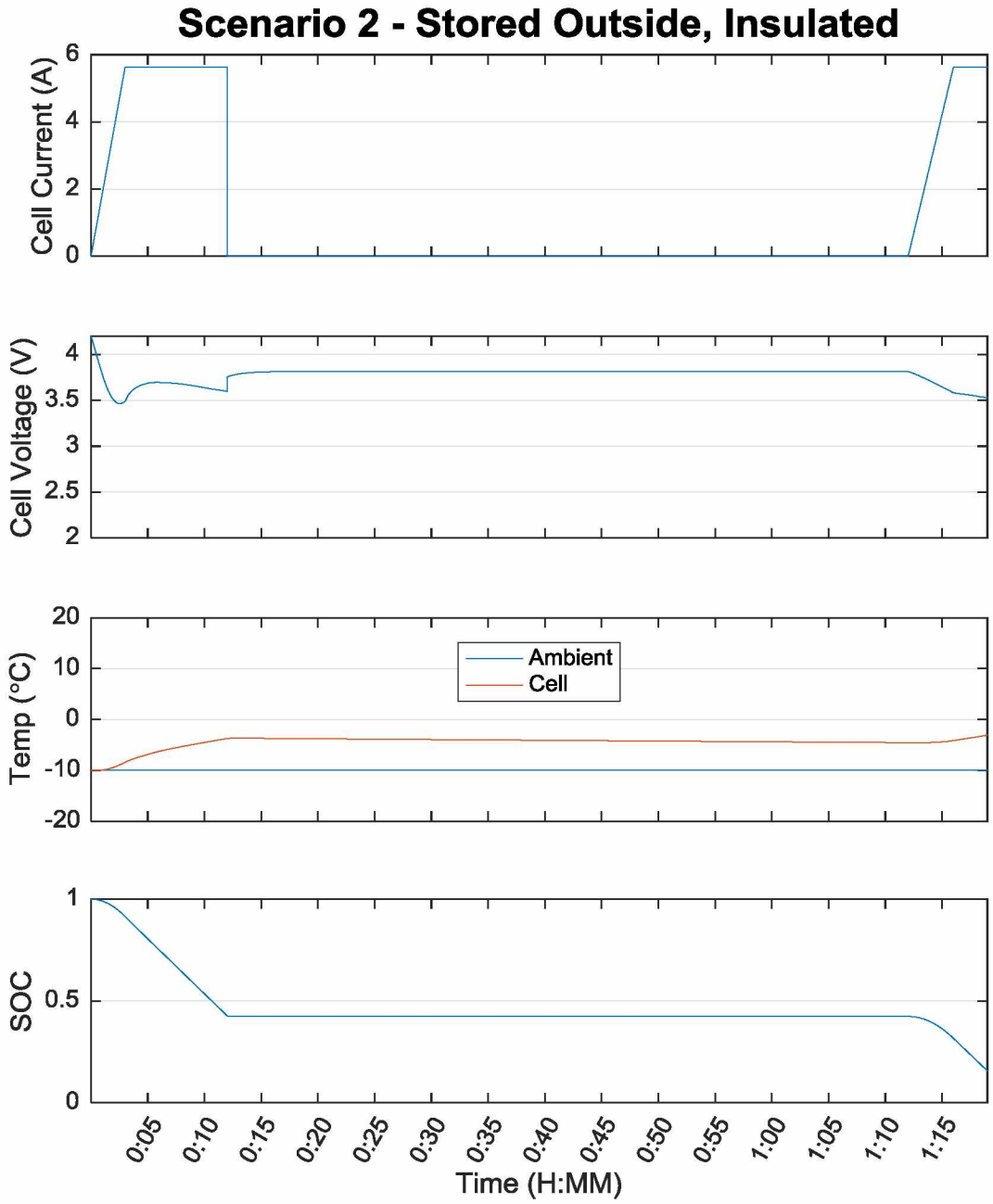

Figure 4-18: Model-based scenario simulating battery pack insulated with 2" of foam. Initial battery temp was set to ambient -10 °C. Cell voltage and temperature were monitored as discharge current was applied. Total energy delivered was calculated to be 5.27 Wh.

Finally, the combined effects of starting with a warm and insulated battery pack were explored. Figure 4-19 shows that storing the battery in a warm environment eliminates the initial dip in voltage, and the insulation keeps the battery warm, with the average battery temperature

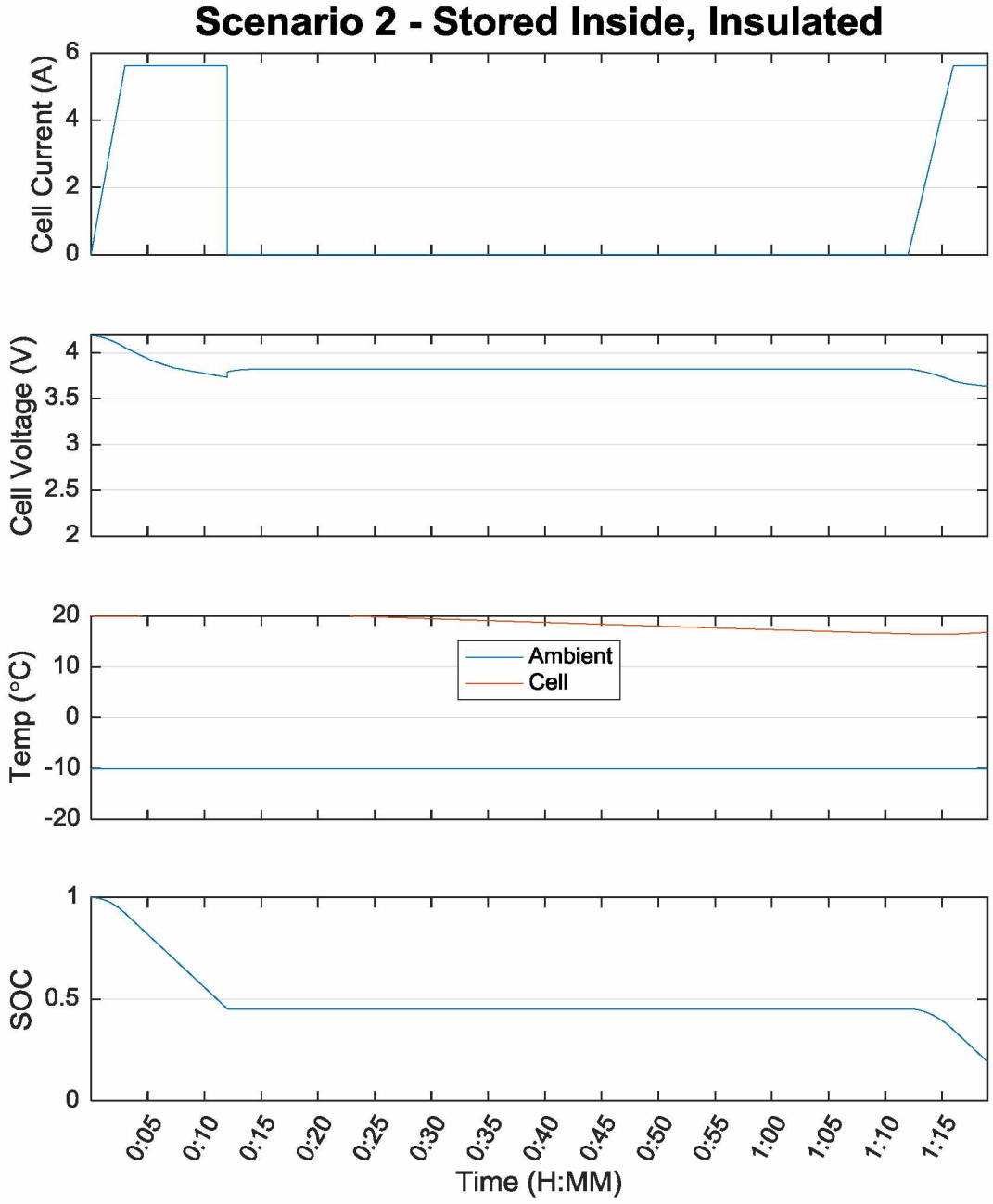

Figure 4-19: Model-based scenario simulating battery pack insulated with 2" of foam. Initial battery temp was set to 20 °C. Cell voltage and temperature were monitored as discharge current was applied. Total energy delivered was calculated to be 5.57 Wh.

dropping less than 5 °C over a one hour period and an initial temperature difference of 30 °C between the battery and ambient. The total energy delivered was 5.57 Wh, versus 5.14 Wh for a cold, non-insulated battery.

4.4 Observations

Three distinct observations can be made from the measured and model-simulated results. First, voltage dips greatly under load when the cells are cold. Second, cell temperature rapidly increases when the cell is under load, which brings the cell closer to nominal performance. Finally, it was observed that without insulation, cell temperature approaches ambient temperature within an hour, if the battery is not subjected to a load.

4.5 Measured Results for Model Validation

The measured results for model validation show both expected and new results for cold weather applications of $LiCo0_2$ cells. The first is that cell performance is largely unaffected by temperature above 0 °C. Performance diminishes with decreasing temperature below 0 °C, with effects of temperature easily seen by -10 °C. It was observed that the lowest practical temperature for non-insulated $LiCo0_2$ cells was -20 °C. This was attributed to an exponential increase in cell internal resistance at temperatures from 0 °C to -20 °C. A single test at -30 °C was attempted but not logged, as internal resistance was reported to be greater than 20 Ω per cell, for a 1.8 Ah cell, at a current rate of 100 mA. The test, which was designed to last 20 hours, lasted less than 5 minutes.

For temperatures above -20 °C, cell self-heating is a factor that definitely needs to be considered. At temperatures where the battery pack is usable, the cells gain heat much faster than they dissipate it, even without insulation. Because of this self-heating, much more energy and power capacity is available if the cells are subjected to a sustained load (where self-heating can maintain internal battery temperatures) rather than being used intensely for short periods of time and then allowed to cool over longer periods of time.

4.6 Modeled Scenario Results

The model results showed the positive effects of both storing the battery in a warm environment before use in the cold, as well as insulating the battery pack. Each was investigated

in turn. For a battery that will be used soon after being subjected to the cold, storing the battery inside a warm garage had the greatest benefit on battery performance due to the lower initial dip in cell voltage. When the cells are operated after cold soaking (outside storage in the winter months), there is a large initial dip in cell voltage before self-heating warms the battery and the voltage rises.

For a battery that will sit for an extended period outside before being used, insulating the battery had the largest effect. For temperatures between -20 °C and 0 °C, insulation will have a positive effect on cell performance. It was observed that the cells produce enough heat during the first 20% of discharge (from SOC = 1 to SOC = 0.8) to bring the performance up to nominal levels. By insulating the cells, this heat will be maintained, rather than lost. In this case, battery performance and energy delivery at -10 °C can match nominal 20 °C performance for the remaining 80% of the discharge cycle.

4.7 Effect of Discharge Rate

Discharge rate (how quickly the cell is discharged) did not appear to affect these cells at temperatures warmer than 0 °C at the tested discharge rates. The cells are rated for 65 C-rate continuous discharge and 130 C-rate peak discharge, and the tests conducted in this thesis did not exceed 3 C-rate. It is likely that the cells would lose their ability to maintain voltage under load if they were tested at the extreme end of their performance window.

For extremely low discharge rates, on the order of 1/1000 C-rate, internal resistance would play a much smaller role in the overall discharge circuit and the cell should be able to supply near-rated energy capacity at temperatures near -20 °C and possibly even colder. However, discharge currents of these magnitudes were not tested in the environmental chamber.

Finally, in Chapter 5, overall conclusions are drawn from the measured and modeled results. In addition, ways to maximize the useful energy available from a given battery pack are discussed, as well as future work which still needs to be done before these $LiCoO_2$ cells can be utilized to power a small electric vehicle for use immediately following severe cold-soaking.

Chapter 5: Conclusions and Future Work

5.1 Scientific Contributions of This Thesis

A number of interesting conclusions were drawn about cold weather operation of lithium polymer batteries from the observations during the testing, measurement and modelling portions of this thesis. As the results showed, there is a definite correlation between temperature and available cell energy at temperatures below the freezing point. However, there are several methods to alleviate this, and these methods can be used individually or in combination to greatly increase battery capability for a given chemistry at a given temperature.

The results of this thesis illustrate that the largest and most detrimental effect on the cells at low temperatures can be attributed almost entirely to increased internal resistance of the cell. The slightly lower value for Ahs extracted from the cell is mostly due to the cell reaching the pre-defined cut-off voltage earlier in the cycle, which is due to the increased voltage drop across the internal resistance of the cell. The lower energy delivered (in Whs) can also be attributed to increased internal resistance, as more of the total energy produced by the electrochemical activity of the cell is converted to heat before it can be used to do useful work.

These results indicate that if a battery pack is appropriately sized (big enough), so that the load current per cell is limited to a small value during use rather than operated at the upper end of the manufacturer suggested range, and if the cells are insulated from the environment, the battery will be able to perform acceptably across the entire temperature range from -20 °C to 20 °C.

5.1.1 Methods to Achieve Higher Battery Energy Output

5.1.1.1 Insulation

Insulating the cells is a very economical way to get more performance from the same cell chemistry. Initial cell performance is still highly affected by ambient temperature, but cell performance can recover to near-nominal long before the full charge is depleted.

5.1.1.2 Larger capacity (more cells)

Increasing the number of cells in the battery pack is another effective method to get more performance from the same cell chemistry. It is easy to imagine that doubling the physical size

and capacity of the battery will double the available energy. In most cases though, the performance gain is actually much greater than double. This is because for a given load current, the load per cell is halved if the capacity is doubled. Since cell losses scale with the square of current rather than linearly, cutting cell current by ½ can decrease cell losses due to internal heating by 75%. By this effect, energy delivery capability of the pack is increased in a better than linear factor as pack capacity is increased. I.e., doubling battery pack capacity will more than double the useable range of the vehicle.

If cell chemistry changes are considered in addition to physical pack changes, the gain can be even greater, because for a given price and size of cell, a trade off can be made to use a cell with a higher energy density but lower power density. Because of the larger pack size there are more cells available to do the work and the per cell power density can be proportionally lower.

5.1.1.3 Warm storage

By storing the machine and battery pack inside, the battery is able to start at a warm temperature, rather than suffering performance loss caused by a cold battery before self-heating warms the pack.

5.1.1.4 Sustained load

As shown in Chapter 4, cell self-heating is a factor that definitely needs to be considered. At temperatures where the battery pack is usable, the cells actually gain heat much faster than they dissipate it, even without insulation. Because of this self-heating, much more energy and power capacity is available if the cells are subjected to a sustained load (where self-heating can maintain internal battery temperatures) rather than being used intensely for short periods and then allowed to cool for long periods.

5.1.2 Operating Cells Outside of Manufacturer Specified Limits

For any lithium battery there is a specified voltage window, given by the manufacturer which according to conventional theory, the cell should always be operated inside of. In addition to current limits and maximum charge voltages, any reputable manufacturer will also list a minimum voltage which the cell should never be discharged below. Under normal conditions and operating temperatures, discharging the cell below this minimum specified voltage will result in permanent damage to the cell. These damaging effects include puffed or bloated cell casings,

greatly increased internal resistance, increased self-discharge rate, and reduced energy storage capacity. These changes are caused by irreversible changes in the cell chemistry.

What was discovered during the research for this thesis is that monitoring terminal voltage only tells part of the story. The important voltage to track is E_m, but without a cell model and knowledge of model topology and component values, this is not possible to measure. During testing at extreme cold temperatures, terminal voltage was repeatedly taken lower than 1 Vdc/cell, without observable negative side effects. The reason this is possible at low temperatures, but not at normal operating temperatures, is due to internal resistance. At low temperatures, the internal resistance is greatly increased and is responsible for most of the terminal voltage drop when the cell is under load. In this way, terminal voltage can be observed to drop well below the manufacturer suggested minimum value, while keeping E_m at a safe operating voltage.

5.1.3 Terminal Voltage Rises under Load

Throughout testing, it was demonstrated that cell voltage can rise under load. This goes against the common understanding of lithium cells, and batteries in general, where voltage is higher for a charged cell and lower for a discharged cell. While it was demonstrated that open circuit cell voltage does indeed decrease for each decrease in SOC, voltage under load appears artificially low when cells are cold due to increased internal resistance. As cell temperature rises due to self-heating, internal resistance drops, and terminal voltage of the loaded cell rises as the cell discharges.

5.1.4 Perceived Capacity Loss Primarily Due to Increased Internal Resistance

Throughout testing, it was observed that the cell maintained its energy capacity throughout the usable and tested temperature range of -20 °C to 20 °C. Reported capacity at low temperatures can artificially appear diminished due to two factors. The first is that internal resistance of the cell causes some of the cell energy to go into self-heating, rather than doing useful work. The second is that for most systems using lithium batteries, end-of-discharge is signaled by the cell reaching a pre-defined minimum value. At low temperatures, and high loads, this voltage floor is reached much sooner because a large percentage of the available cell voltage is dropped across internal resistance. When the load is removed, cell voltage recovers.

5.2 Future Work

5.2.1 Improved Parameter Estimation

Future work would include improvements to the measurement methods and modelling of the actual lithium polymer cell parameters. Better ways to faster-estimate the values for LUTs during the first 20% SOC from SOC = 1 to SOC = 0.8 should be explored. A discharge graph that takes two days per temperature point to acquire is not convenient for cell modeling. Additionally, the method used in this thesis of mapping values at temperatures lower than the desired point and then matching values manually was labor intensive, but still faster than discharging the battery slowly enough to eliminate self-heating. Furthermore, the use of a Kalman filter could help to better estimate model component values. The filter could use known ambient temperatures for initial guesses and update the heating value based on the cell current.

5.2.2 Better Advantage of Cell Self-Heating

Another topic to look at in the future is use of a non-resistive active load to cycle current in and out of the cells, taking advantage of the internal resistance to heat the cells from the inside. An inductive load could be switched through an H-bridge to discharge the cells during a pulse, and then the stored energy in the inductor could be switched and directed back into the battery to recharge the cells. In this way, cell energy could be used to directly heat the battery pack, with very little energy losses outside of the battery pack.

Additionally, it would be worth looking at how much waste heat is generated by the electric motor, and using that waste heat to help warm the batteries, in conjunction with insulation. By this same token, a hybrid vehicle utilizing a very small internal combustion engine as a means of providing some make-up energy to the cells, as well as using the waste heat from the engine to heat the batteries, might be a viable approach. In this scenario the engine would likely be sized based on heat output, choosing an engine that provides only enough waste heat to keep the batteries at an optimal temperature, using the electrical output from the engine as merely a supplement to the battery charge and not enough to directly drive the machine.

5.2.3 Real-World BMS

Finally, it would be advantageous to implement and test (in the real world) some of these strategies for improving the cold weather performance of lithium polymer batteries in small

electric vehicle applications. This could be accomplished by integrating cold temperature models of the batteries into BMSs such as the LTC680x line of ICs. This could also include an active system for distributing charge between cells.

In such a system, a micro controller could be employed to store the cell parameter lookup tables as well as accept inputs from the cell voltage and temperature monitors and load current sensor. The BMS, encompassing the microcontroller, would then be responsible for calculating real-time values for E_m to ensure the cells were operated within the safe operating region. It would also be capable of signaling the motor controller to reduce or limit load current when internal resistance was higher than a pre-defined amount, as would occur with a cold battery pack.

5.3 Closing Thoughts

Though many useful observations and discoveries were made throughout the course of this research, there is still a lot of work to be done in this field. Specifically, the testing, measuring, and modeling done for this thesis identified cell internal resistance as being the primary factor in reduced cell performance at low temperatures, but did not touch on any chemistry changes which would improve this. As battery powered vehicles become commonplace, it will be necessary to develop and implement a battery management strategy which takes these factors into consideration and fully addresses the use of compact, lightweight batteries at temperatures of -20 °C and colder.

References

[1] C. H. Clark, "Primary batteries," *Electrical Engineering,* vol. 69, no. 6, pp. 515-518, 1950.

[2] A. H. Bauer, "Secondary Batteries for Light and Power," *Transactions of the American Institute of Electrical Engineers,* vol. III, no. 1, pp. 129-157, 1886.

[3] K. Mikhaylov and J. Tervonen, "Experimental Evaluation of Alkaline Batteries's Capacity for Low Power Consuming Applications," in *2012 IEEE 26th International Conference on Advanced Information Networking and Applications*, 2012, pp. 331-337.

[4] H. Keshan, J. Thornburg, and T. S. Ustun, "Comparison of lead-acid and lithium ion batteries for stationary storage in off-grid energy systems," in *4th IET Clean Energy and Technology Conference (CEAT 2016)*, 2016, pp. 1-7.

[5] P. G. Horkos, E. Yammine, and N. Karami, "Review on different charging techniques of lead-acid batteries," in *2015 Third International Conference on Technological Advances in Electrical, Electronics and Computer Engineering (TAEECE)*, 2015, pp. 27-32.

[6] S. F. Pensabene and J. W. Gould, "Batteries: Unwanted memory spooks nickel-cadmium cells: New understanding of an undesirable phenomenon is the first step in avoiding it," *IEEE Spectrum,* vol. 13, no. 9, pp. 33-37, 1976.

[7] J. P. Aditya and M. Ferdowsi, "Comparison of NiMH and Li-ion batteries in automotive applications," in *2008 IEEE Vehicle Power and Propulsion Conference*, 2008, pp. 1-6.

[8] M. M. Hoque, M. A. Hannan, and A. Mohamed, "Optimal CC-CV charging of lithium-ion battery for charge equalization controller," in *2016 International Conference on Advances in Electrical, Electronic and Systems Engineering (ICAEES)*, 2016, pp. 610-615.

[9] X. Wu, Z. Mei, C. Hu, C. Zhu, and J. Sun, "Temperature Performance Comparative Analysis of Different Power Batteries," in *2016 IEEE Vehicle Power and Propulsion Conference (VPPC)*, 2016, pp. 1-6.

[10] P. Flowers, K. Theopold, and R. Langley. (2016, 3/22/18). *Batteries and Fuel Cells*. Available: https://chem.libretexts.org/LibreTexts/Valley_City_State_University/Chem_115/Chapter_6%3A_Redox_Chemistry/6.7%3A_Batteries_and_Fuel_Cells

[11] Battery University. (March 1). *Types of Lithium-ion Batteries*. Available: http://batteryuniversity.com/learn/article/types_of_lithium_ion

[12] F. P. Tredeau, B. G. Kim, and Z. M. Salameh, "Performance evaluation of Lithium Cobalt cells and the suitability for use in electric vehicles," in *2008 IEEE Vehicle Power and Propulsion Conference*, 2008, pp. 1-5.

[13] M. Yazdanpour, P. Taheri, A. Mansouri, and M. Bahrami, "A Distributed Analytical Electro-Thermal Model for Pouch-Type Lithium-Ion Batteries," *Journal of the Electrochemical Society,* vol. 161, no. 14, pp. A1953-A1963, 2014.

[14] V. H. Johnson, A. A. Pesaran, and T. Sack, "Temperature-Dependent Battery Models for High-Power Lithium-Ion batteries," presented at the 17th Annual Electric Vehicle Symposium, Quebec, CA, 2001.

[15] O. Erdinc, B. Vural, and M. Uzunoglu, "A dynamic lithium-ion battery model considering the effects of temperature and capacity fading," in *2009 International Conference on Clean Electrical Power*, 2009, pp. 383-386.

[16] W.-Y. Chang, "The State of Charge Estimating Methods for Battery: A Review," *ISRN Applied Mathematics,* vol. 2013, p. 7, 2013, Art. no. 953792.

[17] M. Mastali, J. Vazquez-Arenas, R. Fraser, M. Fowler, S. Afshar, and M. Stevens, "Battery state of the charge estimation using Kalman filtering," *Journal of Power Sources,* vol. 239, pp. 294-307, 2013.

[18] B. G. Kim, D. D. Patel, and Z. M. Salameh, "Circuit Model of 100 Ah Lithium Polymer Battery Cell," *Journal of Power and Energy Engineering,* vol. 01, no. 06, pp. 1-8, 2013.

[19] X. Lin, A. G. Stefanopoulou, Y. Li, and R. D. Anderson, "State of charge estimation of cells in series connection by using only the total voltage measurement," in *2013 American Control Conference*, 2013, pp. 704-709.

[20] N. H. Kutkut, H. L. N. Wiegman, D. M. Divan, and D. W. Novotny, "Charge equalization for an electric vehicle battery system," *IEEE Transactions on Aerospace and Electronic Systems,* vol. 34, no. 1, pp. 235-246, 1998.

[21] C.-H. Kim, M.-Y. Kim, and G.-W. Moon, "A Modularized Charge Equalizer Using a Battery Monitoring IC for Series-Connected Li-Ion Battery Strings in Electric Vehicles," *IEEE Transactions on Power Electronics,* vol. 28, no. 8, pp. 3779-3787, 2013.

[22] S. S. Zhang, K. Xu, and T. R. Jow, "The low temperature performance of Li-ion batteries," *Journal of Power Sources,* vol. 115, no. 1, pp. 137-140, 2003.

[23] Y. Ji, Y. Zhang, and C. Y. Wang, "Li-Ion Cell Operation at Low Temperatures," *Journal of the Electrochemical Society,* vol. 160, no. 4, pp. A636-A649, 2013.

[24] V. Ramadesigan, P. W. C. Northrop, S. De, S. Santhanagopalan, R. D. Braatz, and V. R. Subramanian, "Modeling and Simulation of Lithium-Ion Batteries from a Systems Engineering Perspective," *Journal of the Electrochemical Society,* vol. 159, no. 3, pp. R31-R45, 2012.

[25] A. Nikolian *et al.*, *Classification of Electric modelling and Characterization methods of lithium ion batteries for vehicle applications*. 2016.

[26] F. Jin, H. Yongling, and W. Guofu, "Comparison Study of Equivalent Circuit Model of Li-Ion Battery for Electrical Vehicles," *Research Journal of Applied Sciences, Engineering and Technology,* vol. 6, pp. 3756-3759, 2013.

[27] T. Huria, M. Ceraolo, J. Gazzarri, and R. Jackey, "High fidelity electrical model with thermal dependence for characterization and simulation of high power lithium battery cells," in *2012 IEEE International Electric Vehicle Conference*, 2012, pp. 1-8.

[28] H. He, R. Xiong, and J. Fan, "Evaluation of Lithium-Ion Battery Equivalent Circuit Models for State of Charge Estimation by an Experimental Approach," *Energies,* vol. 4, no. 12, pp. 582-598, 2011.

[29] H. G. Schweiger *et al.*, "Comparison of several methods for determining the internal resistance of lithium ion cells," *Sensors (Basel),* vol. 10, no. 6, pp. 5604-25, 2010.

Appendices

Appendix A. West Mountain Radio CBA IV Pro Specifications

- One model for all testing ranges *
- Maximum continuous discharge rate: 100 watts
- Maximum limited term discharge rate with < 3500 ma-hour battery: 125 watts
- Maximum limited term discharge rate with < 1000 ma-hour battery: 150 watts
- 0-3 amp accuracy: typically better than + - 10 ma
- 3-40 amp accuracy: typically better than + - 45 ma
- 0-5 volt accuracy: typically better than + - .005 volts
- 5-15 volt accuracy: typically better than + - .01 volts
- 10-60 volt accuracy: typically better than + - .05 volts
- Maximum operating voltage: 55 Volts (48 Volt Lead Acid Telecom supported)
- Maximum discharge rate: 40 amps (Battery dependent, 100 watt continuous)
- Minimum discharge voltage to maintain 30 amps .9Volts (Battery dependent)
- Minimum Voltage for a 40 amp discharge: 2 volts at completion of test (Battery dependant)
- Minimum discharge rate: 0.01 Amps *
- Residual current drain, battery connected while not in use: < .003 amps @ 12 volts
- High performance micro controller with built in USB interface and 12 bit A/D conversion.
- USB powered; the CBA does not use the battery being tested to run the CBA or the fan.
- System ready and Test in progress LED indicators, viewable from across a room.
- CBA internal over temperature sensing and protection.
- Graph printing on any standard color or B&W printer.
- Battery test label printing on standard 05160 stick-on labels.
- Dimensions: 3.5" H x 2.8" W x 3.6" D.
- Weight: 16 oz.
-
- * - Improvement/Enhancement over CBA IV

Appendix B. Link to raw data and model files

https://github.com/isaacAlaska/licoo2_cell_data